mathematics

MDPI

Article

A Coupled Laplace–Bessel Approach for Transient and Steady-State Analysis of Multi-Stage Wireless Sensor Networks

Harshini Krishnan [1], Lavanya Gowrishankar [1,*], Anbazhagan Neelamegam [2], Srijana Acharya [3] and Bhanu Shrestha [4,*]

[1] Department of Mathematics, College of Engineering and Technology, SRM Institute of Science and Technology, Kattankulathur, SRM Nagar, Chengalpattu District, Chennai 603203, Tamilnadu, India; hk9665@srmist.edu.in
[2] Department of Mathematics, Alagappa University, Karaikudi 630003, Tamilnadu, India; anbazhagann@alagappauniversity.ac.in
[3] College of Global Business, Kyungsung University, Busan 48434, Republic of Korea; srijana80@ksu.ac.kr
[4] Department of Information Convergence System, Graduate School of Smart Convergence, Kwangwoon University, Seoul 01897, Republic of Korea
* Correspondence: lavanyagowrishankar@yahoo.co.in (L.G.); bnu@kw.ac.kr (B.S.)

Abstract

In this paper, we consider a multi-stage network with transition between intermediate states and relate it to packet movement in wireless sensor networks. Both transient-state and steady-state analyses are carried out. A continuous-time Markov chain model is employed for analysis. The model best resembles a network that can be used to study transient behavior in a packet-switched network, for example, routers in the internet backbone. The state probabilities are analytically derived and numerically computed. The transient-state analysis section explores the system probability in various states. In addition, we explore the average number of packets at a particular time and at a particular state. The transient-state and steady-state solutions help to identify retransmission after a failed attempt, allowing us to study the influence of wireless channel quality. Transition entropy is employed to quantify the uncertainty and dynamic variability in state transitions of the system. Finally, numerical illustrations are provided in order to visualize the network behavior, especially the intensity of data traffic over a time period t. The numerical section captures the transient packet dynamics and evaluates the mean and variance of the packet population. Sensitivity analysis is also performed, showing that higher phase-wise arrival rates increase packet count variability, while experiments with synthetic event logs demonstrate the model's applicability for parameter estimation.

Keywords: continuous-time Markov chain; matrix-geometric method; quasi-birth-and-death process; transient analysis; steady-state analysis; sensitivity analysis

MSC: 60J27; 60K25

Check for updates

Academic Editors: Oleg Tikhonenko and Marcin Ziółkowski

Received: 21 August 2026
Revised: 16 October 2026
Accepted: 19 October 2026
Published: 27 October 2026

Copyright: © 2026 by the authors. Licensee MDPI, Basel, Switzerland. This article is an open access article distributed under the terms and conditions of the Creative Commons Attribution (CC BY) license.

1. Introduction

Wireless sensor networks (WSNs) form an integral part of efficient data transmission, particularly in dynamic environments where packet movement must be optimized. In this study, a multi-stage network model incorporating intermediate state transitions is developed to analyze packet flow in WSNs. The model employs continuous-time Markov chains (CTMC) to investigate both steady-state and transient-state behaviors, providing insights into packet retransmission, delay variations, and the impact of wireless channel quality. The system considers various node states, including active sensing, congestion handling,

relay transmission, and recovery from interference, thereby ensuring a realistic depiction of network behavior. By analytically deriving and numerically computing state probabilities, the model evaluates the temporal evolution of packet movement. This framework is particularly relevant for packet-switched networks such as internet backbone routers and large-scale WSN deployments.

The remaining sections of the paper is organized as follows. Section 1 gives the brief introduction of the paper, while Section 1.1 gives the motivation for the study in two subsections, laying out the theoretical motivation and practical motivation. A literature survey is given in Section 1.2, organized under four subsections: Markov chain-based WSN modeling and MAC-layer analysis; WSN routing, congestion control, reliability and energy management; WSN architectures and application domains; and the queueing model and transient analysis. The model description is given in Section 2, with Section The Quasi-Birth-and-Death (QBD) Process describing the Quasi-Birth-and-Death (QBD) process. The transient analysis is described in Section 3, which has the following subsections: transient-state analysis and hybrid transform representation; governing equation; block QBD representation; Laplace transform of the entry-buffer phase; and matrix–Bessel kernel for the four-phase propagation subsystem. Section 4 gives the steady-state analysis. Section 5 provides an extensive numerical illustration with five subsections: transient state analysis; variance of packets; overall insights and model novelty; steady-state solution; and rate matrix transition entropy. The WSN model of proposed grid is given in Section 7. Conclusions and future work are provided in Section 8 and Section 9, respectively. Finally, the appendices provide in-depth explanations for the parameter estimation formulae along with a detailed computational algorithm.

1.1. Motivation

1.1.1. Theoretical Motivation

Theoretical analysis of wireless sensor networks requires a model that captures stochastic packet arrivals, multistage transmission, retransmission after failures, and feedback between communication stages. Classical single-stage queuing models do not adequately describe these interacting mechanisms. Therefore, the proposed continuous-time Markov chain represents both the number of packets in the system and their current transmission stage. The transient solution provides time-dependent state probabilities for examining short-term traffic evolution, while the matrix-geometric method characterizes the long-run stability and stationary packet distribution. In addition, transition entropy measures the uncertainty in packet movements among network states. This provides an analytical indicator of routing variability and retransmission behavior.

1.1.2. Practical Motivation

In a real wireless sensor network, packets may experience delay, congestion, failed transmission, retransmission, relay forwarding, or alternate routing because of channel errors and changing traffic conditions. The proposed multistage model represents these packet movements through intermediate states and enables the evaluation of packet congestion over time. The transient measures identify temporary traffic peaks and the probability of packets remaining in particular transmission stages, whereas the steady-state measures determine whether the network can handle the offered traffic without excessive queue buildup. Transition entropy further identifies communication stages with highly uncertain packet movement. Hence, the model can assist in designing reliable and stable wireless sensor, relay, and packet-switched communication networks.

1.2. Literature Survey

Studies of wireless sensor networks (WSNs) have extensively employed Markov-chain and queuing-theoretic approaches to investigate packet transmission, routing, congestion, reliability, energy efficiency, and network performance. Recent research has further emphasized transient and steady-state analysis, matrix-analytic methods, delay modeling, and stochastic routing mechanisms. The following literature review covers these developments and identifies their relevance to the proposed multi-stage CTMC-based WSN model.

1.2.1. Markov Chain-Based WSN Modeling and MAC-Layer Analysis

Markov chain models have been widely employed to study the operational dynamics, reliability, and resource utilization of wireless sensor networks (WSNs). Manideep Yenugula [1] investigated Markov chain-based optimization for WSNs, with emphasis on quality of service (QoS), energy efficiency, and real-time decision-making. The study considered an enhanced TDMA–CSMA hybrid protocol that adaptively adjusts time slots and collision avoidance mechanisms to improve communication reliability in Internet of Things (IoT), smart city, and industrial automation applications. Deepakraj and Raja [2] proposed a Markov chain model for energy-aware routing in WSNs, with adjacent nodes identified using location and residual energy information. Their approach selects energy-efficient routes toward the sink node and is evaluated using energy consumption, delay, and residual energy measures. In a related work, the authors of [3] developed a Markov chain-based model to analyze bandwidth states in ZigBee WSNs for remote monitoring applications. Their study examined the CSMA/CA mechanism at the MAC layer of IEEE 802.15.4 networks by considering system load, interference-induced transmission distortion, packet transmission probability, and channel conditions.

1.2.2. WSN Routing, Congestion Control, Reliability, and Energy Management

Several recent studies have focused on improving routing reliability, congestion control, and energy efficiency in multi-hop WSNs. Ma et al. [4] proposed a hierarchical traffic offloading mechanism for multi-hop heterogeneous cellular WSNs to improve end-to-end reliability. Using Stackelberg game theory and Lyapunov optimization, their approach jointly considers traffic scheduling, queuing delay, and transmission reliability. Simulation results based on a 5G–WiFi environment demonstrated the effectiveness of the mechanism in dynamic multilayer networks. Jayamani et al. [5] employed an N-policy in an $M/M/1$ queuing model to improve energy-saving mechanisms in WSNs. Their analysis examined energy consumption, queue length, server idle periods, and operational cost under different values of N. Bhukya and Annavarapu [6] introduced a hybrid trust-based congestion-aware cluster routing protocol to strengthen both security and congestion control in WSNs. Their method combines K-harmonic means clustering with an enhanced gravitational search algorithm to improve node selection, packet delivery, mobile sink routing, energy efficiency, and throughput. Villordo-Jimenez et al. [7] developed a distance-based queuing model for linear WSNs, with relay packet transmission prioritized according to hop distance from the sink. Their analytical and simulation results showed improvements in packet loss uniformity, throughput, reliability, and scalability. Similarly, Yang et al. [8] proposed a distributed power control method for industrial IoT networks to improve queue stability, throughput, resource allocation, energy efficiency, and QoS compliance.

1.2.3. WSN Architectures and Application Domains

Foundational studies have established the relevance of WSNs in large-scale monitoring, industrial automation, smart grids, and security-oriented applications. Yang [9] discussed the design and application challenges of ZigBee-based WSNs, including energy

consumption, routing, fault tolerance, scalability, and network integration with IoT and industrial systems. Callaway [10] provided a broad overview of WSN architectures, communication protocols, power management, security, electromagnetic compatibility, and scalability issues. Liu [11] investigated WSN applications in smart grids, particularly for energy monitoring, prediction and management. The study also emphasized cybersecurity concerns involving privacy, connectivity, and network security while identifying future directions for improving the reliability of WSN-enabled smart grid systems.

1.2.4. Queuing Models and Transient Analysis

Queuing theory provides an important mathematical basis for analyzing congestion, service delay, packet loss, and system stability in communication networks. Arizono and Takemoto [12] studied an $M/M/1$ single-server queue with balking by extending conventional steady-state analysis through concepts from statistical mechanics. Wang et al. [13] investigated an $M^{[X]}/M/1$ queueing system with multiple vacations and server breakdowns, employing the maximum entropy principle to approximate steady-state queue-length distributions and evaluate system performance measures. Kumar et al. [14] analyzed a multi-server feedback retrial queue with finite waiting capacity and a constant retrial rate. They represented the system as a quasi-birth-and-death (QBD) process, derived stability conditions and performance measures using the matrix-geometric method, and developed a procedure for evaluating the busy period. Ammar [15] studied $M/M/1$ queues with impatient customers and multiple vacations, obtaining explicit expressions for time-dependent state probabilities. Kumara et al. [16] investigated a hybrid arrival single-server queue with individual and state-dependent batch arrivals. Their work included a server switch-off period during idle time and derived transient-state probabilities, first-passage time densities, moments, time-dependent performance measures, and steady-state results under suitable stability conditions. Karthick et al. [17] used simulation-based transfer function modeling to study transient behavior in a two-heterogeneous-server queuing system. Rubino [18] presented a comprehensive survey of transient analysis in Markovian queueing systems, emphasizing closed-form transient distributions and uniformization techniques for analytical and numerical evaluation.

1.2.5. Matrix-Geometric Method and Analytical Foundation

The matrix-geometric method is a well-established technique for analyzing structured Markov chains, particularly QBD processes arising in queueing and communication systems. Neuts [19], Latouche and Ramaswami [20], and Stewart [21] developed the theoretical framework and computational methods for matrix-analytic modeling of structured stochastic systems. These methods are particularly useful for deriving stationary probability vectors, stability conditions, queue length measures, and other long-run performance indicators in multistage systems.

1.2.6. Recent Studies Related to the Proposed Work

Recent studies have increasingly applied queuing and Markov-based techniques to analyze the dynamic behavior, reliability, energy efficiency, and delay characteristics of wireless sensor networks. Blondia [22] developed a queuing model for an energy-harvesting wireless sensor node, in which the alternation between transmission and sleep modes was represented through a finite-capacity queue with repeated server vacations. The study derived system occupancy and wait time characteristics using an embedded Markov-chain framework. Kempa and Kurzyk [23] investigated the transient queue size distribution of a WSN node operating under a threshold-type power saving strategy. By obtaining a Laplace transform representation of the transient probabilities, they demonstrated the importance of

time-dependent analysis in energy-efficient sensor networks. Blondia [24] further studied end-to-end response times in energy harvesting WSNs with a receiver-initiated MAC protocol by modeling individual nodes as finite-capacity queuing systems and evaluating packet response time characteristics. Abbad et al. [25] proposed a weighted Markov clustering routing protocol that combines residual energy and sensor distribution information to reduce energy consumption and improve network lifetime. Affane et al. [26] employed a hidden Markov model to develop an energy-aware routing strategy for WSNs, showing that stochastic state-based routing mechanisms can support efficient resource utilization and packet transmission. Dudin and Klimenok [27] analyzed an MAP/G/1 queue with inventory as a model of an energy harvesting WSN node, then derived performance characteristics relevant to packet processing and energy availability. Zhang et al. [28] introduced an adaptive N-policy sleep scheduling mechanism and formulated an $M/M/1/C$ queuing model to evaluate packet delay and timely reliability in heterogeneous WSNs. In a subsequent study, Zhang et al. [29] proposed an active queue management scheme with priority scheduling to control packet congestion, delay, and packet loss in WSNs. Shudrenko and Timm-Giel [30] developed a queuing-theoretic and combinatorial framework for estimating end-to-end delays in TSCH-based wireless sensor networks, highlighting the role of analytical modeling in predicting communication latency. More recently, Kumar et al. [31] formulated a continuous-time Markov process for reliability and sensitivity analysis of WSNs and demonstrated how variations in transition parameters influence network reliability measures. Collectively, these studies establish the effectiveness of Markov chain-based and queuing-theoretic approaches for analyzing packet delay, congestion, energy consumption, reliability, and transient behavior in WSNs; however, comparatively limited attention has been given to unified multi-stage CTMC frameworks that simultaneously incorporate transient and steady-state behavior, matrix-geometric analysis, Laplace–Bessel representations, transition entropy, sensitivity analysis, and data-driven parameter estimation, which motivates the proposed model.

1.3. Research Gap and Contribution of the Proposed Model

Although the existing literature addresses energy-efficient routing, congestion control, MAC-layer modeling, queuing behavior, and steady-state performance in WSNs, comparatively limited attention has been given to a unified multi-stage WSN model that simultaneously captures packet arrivals, sensing, transmission, relay forwarding, rerouting, retransmissions, recovery actions, and transient packet dynamics as shown in Table 1. The model does not assume a separate retrial orbit, vacation mechanism, priority discipline, or parallel multi-server structure; rather, it incorporates retransmission and recovery directly into the phase process. The proposed work addresses this gap by formulating the WSN as a structured continuous-time Markov chain with multiple packet processing phases. The matrix-geometric method is employed to investigate steady-state behavior and system stability, while generating function techniques are used to derive time-dependent state probabilities. The analytical results are supported through numerical computation and graphical illustrations. Thus, the proposed model demonstrates how advanced queuing-theoretic tools can be applied to evaluate the reliability, stability, packet dynamics, and operational performance of WSNs.

The main contribution of this work is the development of a architecture-correlated stochastic model that integrates both node-level and system-level dynamics in a multi-stage wireless sensor network (WSN). Unlike existing approaches, this model explicitly couples the population of undelivered packets with the functional communication stages of the network, enabling comprehensive analysis of packet congestion, stage-wise pro-

cessing, relay forwarding, bypass routing, retransmission, and recovery within a unified stochastic framework.

Table 1. Comparison of the proposed model with related studies.

Reference	Main Focus and Approach	Difference from the Present Work
(a) Singh et al. (2026) [32]	Energy efficiency in an unreliable cognitive radio network, using advanced sleep modes, hybrid spectrum access, imperfect sensing, DTMC-based transient analysis, and multi-objective optimization.	The present work does not address cognitive radio spectrum sharing or sleep mode optimization; it develops an architecture-correlated multi-stage WSN formulation in which the joint state $X(t) = (N(t), E(t))$ simultaneously represents the number of undelivered packets and the active packet processing/communication stage.
(b) Champati et al. (2020) [33]	Studies the transient behavior of multi-hop wireless networks under static routing, and derives end-to-end delay and backlog bounds using stochastic network calculus.	The present work resolves the internal communication process into buffering, sensing/processing, wireless transmission, relay forwarding, and recovery/retransmission phases through a CTMC/QBD representation.
(c) Sudhesh and Mohammed Shapique (2022) [34]	Uses a multiple vacation queue with threshold policy for WSN dynamic power management. The main states are busy, wake-up, shutdown, and inactive, with transient and steady-state measures.	In contrast, phases in the present work represent packet processing and communication operations. The state (n, j) jointly represents the number of undelivered packets and the active communication phase.
(d) Bayan and Erfani (2007) [35]	Develops a two-dimensional Laplace transform methodology for linear time-varying systems, leading to Bessel-type differential equations.	In the present work, Laplace–Bessel techniques are used as analytical tools for solving the transient equations generated by the proposed WSN model.
Present work	Develops an architecture-correlated multi-stage CTMC/QBD representation $X(t) = (N(t), E(t))$, where $N(t)$ is the number of undelivered packets and $E(t)$ is the active communication phase.	The main distinction is the hybrid node–system coupling of packet population dynamics with buffering, sensing, transmission, relay forwarding, and recovery/retransmission. Phase-dependent λ^j and μ_j together with forward, backward, direct-forward, and direct-backward transitions couple packet-load evolution with the active communication phase.

Specifically, the WSN communication process is represented as a CTMC combined with a QBD process, defined by the joint state $X(t) = (N(t), E(t)) = (n, j)$. Here, $N(t) = n$ denotes the number of undelivered packets in the source–relay–sink fragment, while $E(t) = j$, $j \in \{0, 1, 2, 3, 4\}$ corresponds to one of five distinct functional stages: entry buffering, sensing/initial processing, wireless transmission, relay forwarding, and recovery/retransmission. This direct correspondence between the physical architecture and the mathematical model provides a structured and interpretable framework with which to comprehensively analyze the system. Phase-dependent packet arrival along with the service rates λ^j and μ_j govern the growth and depletion of the packet population, while transition rates γ_F, δ_B, γ_{DF}, and δ_{DB} respectively model the forward, backward, direct-forward, and direct-backward stage transitions. This detailed transition structure captures complex network behaviors such as congestion and retransmissions in a single model rather than treating these mechanisms separately.

It is important to note that while the matrix-geometric method, Laplace transform techniques, and associated analytical tools are used as solution approaches, they are established methods and are not the primary novelty of this work. Our contribution is in the architecture-aware coupling of packet-level population dynamics and communication stages, which allows for integrated performance evaluation of multi-stage WSNs.

2. Model Description

The proposed network models a wireless sensor network. The states $(n,1)$, $(n,2)$, $(n,3)$, and $(n,4)$ represent the different behaviors of the nodes. The packets enter the network at $(1,0)$ and are passed to $(1,1)$. This node is active and sensing. In case of packet congestion, the packet is transferred to nodes $(2,0)$, $(3,0)$, ..., and so on.

The state variables and their interpretations used throughout the proposed model are summarized in Table 2.

Table 2. Mapping of the CTMC state variables to the physical WSN architecture.

Symbol	Term	Architecture Component	Description
$X(t)$	System process	Entire source–relay–sink fragment	CTMC describing the overall state of the considered WSN communication path at time t.
$N(t)$	Level process	Buffer/communication path	Number of undelivered packets currently present in the considered source–relay–sink fragment.
$E(t)$	Phase process	Communication-stage selector	Indicates the physical communication/processing stage occupied at time t.
$(n,0)$	Entry buffer state	Source node buffer	Packet is stored in the local source buffer before sensing/processing activation.
$(n,1)$	Sensing state	Source sensor node	Source node senses, generates or initially processes the packet.
$(n,2)$	Transmission state	Source transmitter and source–relay link	Packet is transmitted from the source toward the relay.
$(n,3)$	Relay forwarding state	Relay node	Relay receives and forwards the packet toward the sink.
$(n,4)$	Recovery state	Source/relay recovery mechanism	Recovery, retransmission, or alternative forwarding is performed after a transmission or forwarding failure.
–	Successful delivery	Sink node	Successful packet reception terminates the packet's progression through the modeled CTMC.

Node $(n,2)$ transmits the sensing data to the next hop, say, $(n,3)$, that is, the data travel to the additional relay nodes. Node $(n,4)$ can be treated as being in recovery mode, waiting to restore communication due to interference. This redirects the data to node $(n,2)$ or $(n,3)$. If node $(n,3)$ is occupied, it redirects the data to $(n,1)$, $(n-1,3)$, or $(n+1,3)$ for $n \geq 2$. When $n = 1$, the data from node $(n,3)$ may be routed to $(n+1,3)$ or $(n,1)$. Thus, the model attempts to address the bottleneck and channel the data for efficient transition.

In the Markov chain model used for this study, the temporal behavior of the network is depicted by studying how the states change through transitions over time. Here, $(n,0)$ is the starting state; the process moves through the states up to $(n,4)$, where n is countably infinite.

The detailed state representation underpins the dynamic routing strategy, which in turn relies on the Markov chain framework to capture temporal behavior. The scalable grid model ensures that these innovations are applicable to large-scale networks, while the use of real-world parameters enhances the model's practical applicability. This results in predictive capabilities that set the proposed approach apart from traditional reactive methods.

2.1. The Quasi-Birth-and-Death (QBD) Process

The number of jobs in the system at time t is indicated by $N(t)$. Considered as a quasi-birth-and-death process, the state of the system is denoted by

$$X(t) = \{(N(t), E(t)) \mid t \geq 0\}. \tag{1}$$

The phase process $E(t)$ is defined as follows:

$$E(t) = \begin{cases} 0, & \text{packet upload} \\ 1, & \text{initial packet transition} \\ 2, & \text{intermediate node that transmits the data} \\ 3, & \text{additional relay nodes} \\ 4, & \text{node in the recovery mode} \end{cases} \tag{2}$$

where $E(t) = 3$ or 4 indicates either that the data have been transferred to other nearby nodes due to congestion or breakdown, or that the node is in recovery mode; the diagrammatic representation of the network is given in Figure 1. The time-dependent probability $P_{n,j}(t)$ denotes that the system is in state j having n packets at time t the state transitions are depicted in Table 3. The physical interpretation and estimation of the proposed WSN model parameters is given in Table 4.

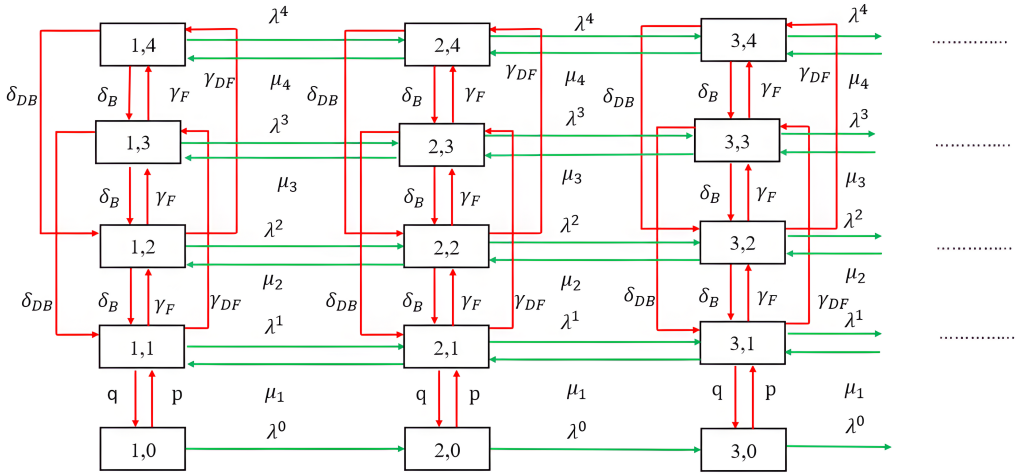


Figure 1. State transition diagram of the proposed WSN model.

Table 3. State-transition directions of the proposed WSN CTMC model.

Transition Rate	State Transition
λ^j	$(n,j) \to (n+1,j), \quad n \geq 1,\ j = 0,\ldots,4$
μ_j	$(n,j) \to (n-1,j), \quad n \geq 2,\ j = 1,\ldots,4$
p	$(n,0) \to (n,1), n \geq 1$
q	$(n,1) \to (n,0), n \geq 1$
γ_F	$(n,j) \to (n,j+1),\ n \geq 1; j = 1,\ldots,4$
δ_B	$(n,j) \to (n,j-1),\ n \geq 1; j = 2,3,4$
γ_{DF}	$(n,j) \to (n,j+2),\ n \geq 1; j = 1,2$
δ_{DB}	$(n,j) \to (n,j-2),\ n \geq 1; j = 3,4$

Table 4. Physical interpretation and estimation of the proposed WSN model parameters.

Parameter	State Transition	WSN Interpretation	Estimation from Packet Traces
λ^j	$(i,j) \to (i+1,j)$	Effective packet arrival or queue growth rate while the system is in phase j, representing an increase in the number of undelivered packets.	$\hat{\lambda}^j = \frac{\sum_i N_{(i,j),(i+1,j)}}{\sum_i T_{(i,j)}}$ s^{-1}
μ_j	$(i,j) \to (i-1,j)$	Effective service or successful clearance rate in phase j due to packet delivery, successful forwarding, or completion of service.	$\hat{\mu}_j = \frac{\sum_i N_{(i,j),(i-1,j)}}{\sum_i T_{(i,j)}}$ s^{-1}
p	$(i,0) \to (i,1)$	Rate at which an arriving packet is activated for sensing or enters the processing stage.	$\hat{p} = \frac{\sum_i N_{(i,0),(i,1)}}{\sum_i T_{(i,0)}}$ s^{-1}

Table 4. *Cont.*

Parameter	State Transition	WSN Interpretation	Estimation from Packet Traces
q	$(i,1) \to (i,0)$	Rate at which an active packet returns to the entry buffer because of deferred sensing, re-buffering, or unsuccessful activation.	$\hat{q} = \frac{\sum_i N_{(i,1),(i,0)}}{\sum_i T_{(i,1)}}$ s^{-1}
γ_F	Forward adjacent-stage transition	Rate of normal stage progression, such as sensing → transmission or transmission → relay forwarding.	Number of successful forward adjacent-stage transitions divided by the total residence time in the originating state.
δ_B	Backward adjacent-stage transition	Rate of local retry or feedback after failure, congestion, or unsuccessful forwarding.	Number of backward adjacent-stage transitions divided by the total residence time in the originating state.
γ_{DF}	Direct-forward bypass transition	Rate of direct forwarding or bypass routing that skips an intermediate stage when an alternate route is available.	Number of direct-forward rerouting events divided by the total residence time in the originating state.
δ_{DB}	Direct-backward bypass transition	Rate of direct backward rerouting, retransmission, or return to an earlier communication stage after interference or link failure.	Number of direct-backward recovery events divided by the total residence time in the originating state.

Using lexicographical sequence for the states, the Markov chain's infinitesimal generator matrix Q is defined as follows:

$$Q = \begin{bmatrix} B_0 & A_0 & 0 & 0 & 0 & \cdots \\ A_2 & A_1 & A_0 & 0 & 0 & \cdots \\ 0 & A_2 & A_1 & A_0 & 0 & \cdots \\ 0 & 0 & A_2 & A_1 & A_0 & \ddots \\ \vdots & \vdots & \ddots & \ddots & \ddots & \ddots \end{bmatrix}. \tag{3}$$

3. Transient-State Analysis

The transient-state analysis aligns with power consumption models employed in duty cycling mechanisms for low-power WSNs. Wireless protocols such as ZigBee, LoRa, and Bluetooth Low Energy use probabilistic approaches, which motivate the study of transient-state analysis mainly to minimize energy consumption. This leads to the development of the following sections.

3.1. Transient-State Analysis and Hybrid Transform Representation

Let

$$X(t) = \{N(t), E(t)\}, \qquad t > 0$$

denote the continuous-time Markov chain describing the proposed multistage system, where

$$N(t) \in \{1, 2, \ldots\}$$

denotes the packet level or the number of undelivered packets and

$$E(t) \in \{0, 1, 2, 3, 4\}$$

denotes the operational phase. The phase $E(t) = 0$ represents the packet entry or buffer state, whereas phases $E(t) = 1, 2, 3, 4$ represent active sensing, transmission, relay routing, and recovery, respectively.

For $n \geq 1$ and $j = 0, 1, 2, 3, 4$, define the transient-state probabilities by

$$P_{n,j}(t) = \Pr\{N(t) = n,\, E(t) = j \,|\, X(0) = (1, 0)\}. \tag{4}$$

The system is assumed to start with one packet in the entry buffer phase. Hence, the initial distribution is given by

$$P_{n,j}(0) = \begin{cases} 1, & (n, j) = (1, 0), \\ 0, & \text{otherwise.} \end{cases} \tag{5}$$

Accordingly,

$$P_{1,0}(0) = 1, \qquad P_{n,0}(0) = 0, \quad n \geq 2$$

and

$$P_{n,j}(0) = 0, \qquad n \geq 1, \quad j = 1, 2, 3, 4.$$

3.2. Governing Equations

Implementing the Chapman–Kolmogorov forward differential-difference equations for the system given in Figure 1, we obtain $P_{n,j}(t)$ as in ref. [16].

$$\frac{dP_{1,0}(t)}{dt} = -(p + \lambda^0)P_{1,0}(t) + qP_{1,1}(t). \tag{6}$$

$$\frac{dP_{n,0}(t)}{dt} = -(p + \lambda^0)P_{n,0}(t) + qP_{n,1}(t) + \lambda^0 P_{n-1,0}(t), \qquad n \geq 2. \tag{7}$$

$$\begin{aligned} \frac{dP_{1,1}(t)}{dt} = & -(\lambda^1 + q + \gamma_F + \gamma_{DF})P_{1,1}(t) + pP_{1,0}(t) + \delta_B P_{1,2}(t) \\ & + \delta_{DB}P_{1,3}(t) + \mu_1 P_{2,1}(t). \end{aligned} \tag{8}$$

$$\begin{aligned} \frac{dP_{n,1}(t)}{dt} = & -(\lambda^1 + q + \gamma_F + \gamma_{DF} + \mu_1)P_{n,1}(t) + pP_{n,0}(t) + \delta_B P_{n,2}(t) \\ & + \delta_{DB}P_{n,3}(t) + \mu_1 P_{n+1,1}(t) + \lambda^1 P_{n-1,1}(t), \qquad n \geq 2. \end{aligned} \tag{9}$$

$$\begin{aligned} \frac{dP_{1,2}(t)}{dt} = & -(\lambda^2 + \gamma_F + \gamma_{DF} + \delta_B)P_{1,2}(t) + \delta_B P_{1,3}(t) + \gamma_F P_{1,1}(t) \\ & + \delta_{DB}P_{1,4}(t) + \mu_2 P_{2,2}(t). \end{aligned} \tag{10}$$

$$\begin{aligned} \frac{dP_{n,2}(t)}{dt} = & -(\lambda^2 + \gamma_F + \gamma_{DF} + \delta_B + \mu_2)P_{n,2}(t) + \gamma_F P_{n,1}(t) \\ & + \delta_B P_{n,3}(t) + \delta_{DB}P_{n,4}(t) + \mu_2 P_{n+1,2}(t) + \lambda^2 P_{n-1,2}(t), \qquad n \geq 2. \end{aligned} \tag{11}$$

$$\begin{aligned} \frac{dP_{1,3}(t)}{dt} = & -(\lambda^3 + \delta_B + \gamma_F + \delta_{DB})P_{1,3}(t) + \gamma_F P_{1,2}(t) + \delta_B P_{1,4}(t) \\ & + \gamma_{DF}P_{1,1}(t) + \mu_3 P_{2,3}(t). \end{aligned} \tag{12}$$

$$\begin{aligned} \frac{dP_{n,3}(t)}{dt} = & -(\lambda^3 + \delta_B + \gamma_F + \delta_{DB} + \mu_3)P_{n,3}(t) + \gamma_F P_{n,2}(t) \\ & + \delta_B P_{n,4}(t) + \gamma_{DF}P_{n,1}(t) + \mu_3 P_{n+1,3}(t) + \lambda^3 P_{n-1,3}(t), \qquad n \geq 2. \end{aligned} \tag{13}$$

$$\begin{aligned} \frac{dP_{1,4}(t)}{dt} = & -(\lambda^4 + \delta_{DB} + \delta_B)P_{1,4}(t) + \gamma_F P_{1,3}(t) \\ & + \gamma_{DF}P_{1,2}(t) + \mu_4 P_{2,4}(t). \end{aligned} \tag{14}$$

$$\begin{aligned}\frac{dP_{n,4}(t)}{dt} = & -(\lambda^4 + \delta_{DB} + \delta_B + \mu_4)P_{n,4}(t) + \gamma_F P_{n,3}(t) \\ & + \gamma_{DF}P_{n,2}(t) + \mu_4 P_{n+1,4}(t) + \lambda^4 P_{n-1,4}(t), \qquad n \geq 2.\end{aligned} \tag{15}$$

Equations (6)–(15) constitute a coupled transient system. The coupling occurs within each level through the phase transition rates p, q, γ_F, γ_{DF}, δ_B, and δ_{DB}, and occurs between adjacent levels through the level increase and level decrease rates λ^j and μ_j, respectively, $j = 1, 2, 3, 4$. Consequently, the phase probabilities cannot be evaluated independently.

3.3. Block-QBD Representation

For notational convenience, define the row vector

$$\boldsymbol{\pi}^*_n(t) = \left[P_{n,0}(t), P_{n,1}(t), P_{n,2}(t), P_{n,3}(t), P_{n,4}(t)\right], \qquad n \geq 1. \tag{16}$$

For all interior levels ($n \geq 2$), the coupled system can be expressed compactly as

$$\frac{d\boldsymbol{\pi}^*_n(t)}{dt} = \boldsymbol{\pi}^*_{n-1}(t)A_0 + \boldsymbol{\pi}^*_n(t)A_1 + \boldsymbol{\pi}^*_{n+1}(t)A_2, \tag{17}$$

where A_0, A_1 and A_2 are defined in Equations (A11), (A12), and (A13), respectively.

At the boundary level $n = 1$, the equations take the form

$$\frac{d\boldsymbol{\pi}^*_1(t)}{dt} = \boldsymbol{\pi}^*_1(t)B_0 + \boldsymbol{\pi}^*_2(t)A_2, \tag{18}$$

where

$$B_0 = A_1 + A_2.$$

The boundary block B_0 differs from the interior block because a level decrease transition below $n = 1$ is not permitted in the present state space.

The initial vector is

$$\boldsymbol{\pi}^*_1(0) = (1, 0, 0, 0, 0), \qquad \boldsymbol{\pi}^*_n(0) = \mathbf{0}, \qquad n \geq 2. \tag{19}$$

Since all transition rates are finite and non-negative, the corresponding truncated generator defines a finite-dimensional linear system with a unique solution. For the countably infinite model, under the standard conservative and non-explosion assumptions for continuous-time Markov chains, the transient probability vector is uniquely determined by the forward equations together with the initial distribution in Equation (5).

3.4. Laplace Transform of the Entry Buffer Phase

The entry buffer phase ($j = 0$) has no level decrease transition. The supplementary mathematical details of the generating-function formulation and the Laplace-transform treatment of the entry-buffer phase are presented in Appendix A. Define

$$P(z, t) = \sum_{n=1}^{\infty} P_{n,0}(t)z^n, \qquad |z| \leq 1, \tag{20}$$

and

$$F_1(z, t) = \sum_{n=1}^{\infty} P_{n,1}(t)z^n. \tag{21}$$

Multiplying Equations (6) and (7) by appropriate powers of z and summing over $n \geq 1$ gives

$$\frac{\partial P(z, t)}{\partial t} = \left[\lambda^0 z - (p + \lambda^0)\right]P(z, t) + qF_1(z, t), \tag{22}$$

with

$$P(z, 0) = z.$$

Let

$$\widetilde{P}(z,s) = \int_0^\infty e^{-st} P(z,t)\, dt \tag{23}$$

and

$$\tilde{F}_1(z,s) = \int_0^\infty e^{-st} F_1(z,t)\, dt. \tag{24}$$

Taking the Laplace transform of Equation (22) yields

$$\widetilde{P}(z,s) = \frac{z + q\tilde{F}_1(z,s)}{s + p + \lambda^0 - \lambda^0 z}. \tag{25}$$

Equation (25) shows that the entry buffer probabilities are coupled with the active sensing phase; hence, the phase-0 component cannot be solved independently of the remaining communication phases.

3.5. Matrix–Bessel Kernel for the Four-Phase Propagation Subsystem

The level transition rates of phases $j = 1, \dots, 4$ are the same. Define

$$\mathbf{u}_n(t) = \left[P_{n,1}(t), P_{n,2}(t), P_{n,3}(t), P_{n,4}(t)\right] \tag{26}$$

and let

$$\mathbf{e}_1 = (1,0,0,0).$$

For $n \geq 2$, the four-phase propagation subsystem satisfies

$$\frac{d\mathbf{u}_n(t)}{dt} = \lambda \mathbf{u}_{n-1}(t) + \mathbf{u}_n(t)[C_4 - (\lambda + \mu)I_4] + \mu \mathbf{u}_{n+1}(t) + pP_{n,0}(t)\mathbf{e}_1, \tag{27}$$

where

$$C_4 = \begin{bmatrix} -(q + \gamma_F + \gamma_{DF}) & \gamma_F & \gamma_{DF} & 0 \\ \delta_B & -(\delta_B + \gamma_F + \gamma_{DF}) & \gamma_F & \gamma_{DF} \\ \delta_{DB} & \delta_B & -(\delta_{DB} + \delta_B + \gamma_F) & \gamma_F \\ 0 & \delta_{DB} & \delta_B & -(\delta_{DB} + \delta_B) \end{bmatrix}. \tag{28}$$

The interior part of (27) admits a modified Bessel kernel. Define

$$b_r(t) = e^{-(\lambda+\mu)t}\left(\frac{\lambda}{\mu}\right)^{r/2} I_r\left(2t\sqrt{\lambda\mu}\right), \qquad r \in \mathbb{Z}, \tag{29}$$

where $I_r(\cdot)$ is the modified Bessel function of the first kind of order (r).

The associated matrix–Bessel propagation kernel is

$$K_r(t) = b_r(t)e^{C_4 t}. \tag{30}$$

The kernel in (30) satisfies the interior recurrence associated with (27). Nevertheless, the complete system remains coupled because of the forcing term $pP_{n,0}(t)\mathbf{e}_1$, the feedback transition with rate (q), and the special boundary structure at level $n = 1$. Therefore, the Bessel kernel is used as an auxiliary propagation kernel within a coupled Laplace transform formulation rather than as an independent scalar solution for every phase probability.

3.6. Matrix-Exponential Evaluation and Numerical Validation

For numerical evaluation, the level space is truncated at a sufficiently large level N. Let

$$\mathbf{\Pi}^{(N)}(t) = [\boldsymbol{\pi}_1^*(t), \boldsymbol{\pi}_2^*(t), \dots, \boldsymbol{\pi}_N^*(t)] \tag{31}$$

be the truncated probability vector and let Q_N denote the corresponding finite generator matrix:

$$Q_N = \begin{pmatrix} B_0 & A_0 & 0 & \cdots & 0 \\ A_2 & A_1 & A_0 & \ddots & \vdots \\ 0 & A_2 & A_1 & \ddots & 0 \\ \vdots & \ddots & \ddots & \ddots & A_0 \\ 0 & \cdots & 0 & A_2 & A_1^{(N)} \end{pmatrix}. \tag{32}$$

where $A_1^{(N)} = A_1 + A_0$ is selected according to the specified upper boundary treatment. At the upper boundary,

$$A_2\mathbf{e} + A_1^{(N)}\mathbf{e} = A_2\mathbf{e} + (A_1 + A_0)\mathbf{e} = 0,$$

so the finite generator remains conservative.

The transient solution is obtained from

$$\mathbf{\Pi}^{(N)}(t) = \mathbf{\Pi}^{(N)}(0)e^{Q_N t}, \tag{33}$$

where

$$\mathbf{\Pi}^{(N)}(0) = (1, 0, 0, 0, 0, 0, \ldots, 0).$$

The probabilities computed from (33) provide an independent numerical benchmark for the coupled Laplace–matrix-Bessel representation. In particular, the agreement between the matrix-exponential probabilities and the corresponding simulation estimates confirms that the proposed transient formulation preserves the complete interdependence among entry buffering, sensing, transmission, relay routing, recovery, and level evolution.

Computation Algorithm of the Complete Coupled Transient Probability Vector

Step 1. Specify the model parameters p, q, γ_F, γ_{DF}, δ_B, δ_{DB}, λ^j, and μ_j, the truncation level $N_{\max}$, the time grid $t_0, \ldots, t_K$, and the initial state $X(0) = (1, 0)$.

Step 2. Construct the within-level phase transition matrix C and the QBD blocks B_0, A_0, A_1, and A_2.

Step 3. Establish the Laplace representation of the entry buffer phase and the matrix–Bessel kernel

$$K_r(t) = b_r(t)e^{C_4 t}$$

which characterizes the homogeneous four-phase propagation subsystem.

Step 4. Construct the truncated generator Q_N, where the blocked-arrival upper boundary block is $A_1^{(N)}$

Step 5. Verify the generator conditions $Q_N\mathbf{e} = \mathbf{0}$ and confirm that all off-diagonal transition rates are non-negative.

Step 6. Set the initial probability vector as $\mathbf{\Pi}^{(N)}(0) = (1, 0, \ldots, 0)$.

Step 7. For each required time t_k, compute the complete coupled transient vector:

$$\mathbf{\Pi}^{(N)}(t_k) = \mathbf{\Pi}^{(N)}(0)e^{Q_N t_k}.$$

Step 8. Extract the individual state probabilities using $P_{n,j}(t_k) = \left[\mathbf{\Pi}^{(N)}(t_k)\right]_{5(n-1)+j}$ for $1 \le n \le N_{\max}, j \in \{0, 1, 2, 3, 4\}$.

Step 9. Verify probability normalization, $\sum_{n=1}^{N_{\max}} \sum_{j=0}^{4} P_{n,j}(t_k) \approx 1$ and repeat the calculation for increasing $N_{\max}$ until truncation convergence is achieved.

Step 10. Use the resulting probabilities to compute $E[N(t)]$, $\mathrm{Var}[N(t)]$, phase-wise transient probabilities, and the other reported performance measures.

Note: The Laplace–matrix-Bessel formulation provides the analytical propagation representation of the coupled equations, while the complete reported transient probabilities are numerically evaluated from the equivalent coupled generator through the matrix exponential.

4. Steady-State Analysis

Two different stationary quantities are used in the steady-state analysis. The stationary vector associated with the background phase process is denoted by

$$\boldsymbol{\alpha} = (\alpha_0, \alpha_1, \alpha_2, \alpha_3, \alpha_4),$$

whereas the stationary probability vector associated with packet level n of the full QBD is denoted by

$$\boldsymbol{\pi}_n = (\pi_{n,0}, \pi_{n,1}, \pi_{n,2}, \pi_{n,3}, \pi_{n,4}), \qquad n \geq 1.$$

where $\pi_{n,j}$ represents the long-run probability that the system contains n undelivered packets and is operating in communication phase j.

Following the matrix-geometric approach [20], the stationary level vectors of the proposed QBD are expressed as

$$\boldsymbol{\pi}_n = \boldsymbol{\pi}_1 R^{n-1}, \qquad n \geq 1, \tag{34}$$

where R is the rate matrix associated with the block matrices A_0, A_1, and A_2.

The boundary vector $\boldsymbol{\pi}_1$ is obtained from

$$\boldsymbol{\pi}_1 (B_0 + RA_2) = 0 \tag{35}$$

together with

$$\boldsymbol{\pi}_1 (I - R)^{-1} \mathbf{e} = 1. \tag{36}$$

The standard matrix-quadratic equation defining R and the corresponding derivation are provided in the Appendix B.

5. Numerical Illustration

A CTMC model with five phases and N levels can be used to represent a multi-stage communication system such as a WSN. The transient probabilities are calculated for states $j = 0$ to 4 over the interval $t \in [0, 50]$ units, where $p = 0.6$, $q = 0.4$, $\gamma_F = 0.3$, $\gamma_{DF} = 0.3$, $\delta_B = 0.3$, $\delta_{DB} = 0.1$, $\mu_1 = \mu_2 = \mu_3 = \mu_4 = 0.06$, and $\lambda^0 = \lambda^1 = \lambda^2 = \lambda^3 = \lambda^4 = 0.04$. It is evaluated for several initial packet counts $n = 1, 2, 3, 4, 5$. We visualize $P_{n,j}(t)$ for individual states and for a specific level ($n = 1$) to show how the system evolves over time. The numerical parameter values are selected as admissible illustrative values consistent with the transition structure and stability requirements of the proposed CTMC/QBD model, following general numerical analysis practice adopted in related queuing and QBD studies [36,37].

5.1. Transient-State Analysis

This section gives graphical plots explaining the transient probabilities of the system in various states. Figures 2–6 clearly display the transient behaviors of the model, taking into account the transient probabilities $P_{n,j}(t)$. These plots collectively illustrate the movement of the packets across the four operational states and the final recovery state. The analysis is in terms of peak time, peak probability, and transition characteristics. Figures 2 and 3 plot the pattern of $P_{n,0}(t)$ and $P_{n,1}(t)$ versus time t for $n = 1$ to 5. It can be observed that the probability curves start at zero slowly and converge to a steady state after a certain time. Figures 4–6 give insight into when $P_{n,2}(t)$, $P_{n,3}(t)$, and $P_{n,4}(t)$ attain steady state. In addition, state $j = 0$ exhibits purely monotonic decay, indicating immediate exit from the packet upload phase. From the states $j = 1$, $j = 2$, and $j = 3$, transient peaks can be observed with increasing delay and decreasing magnitude. This reflects system congestion and deeper delay traversal. The recovery state has the slowest initial rise and least occupancy, exhibiting fallback behavior.

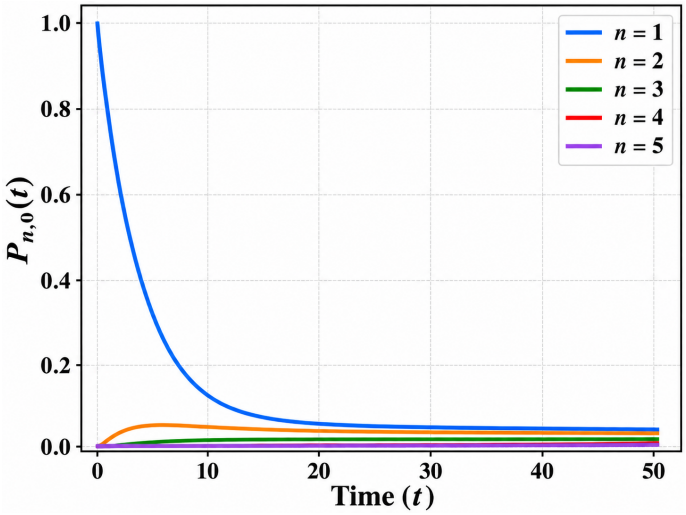


Figure 2. $P_{n,0}(t)$ versus time t.

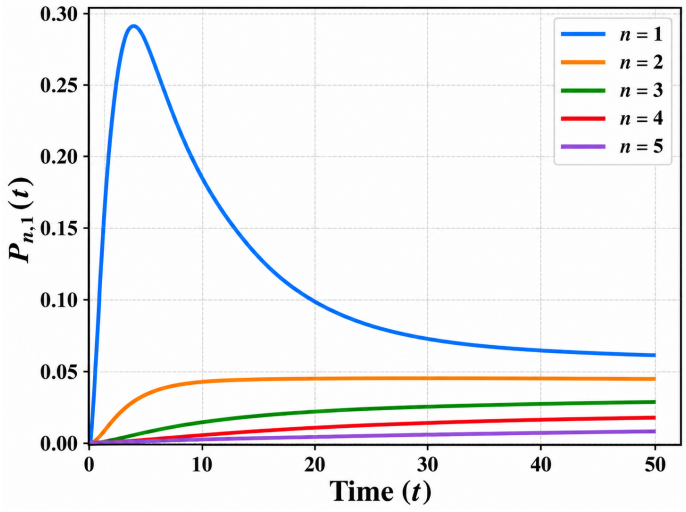


Figure 3. $P_{n,1}(t)$ versus time t.

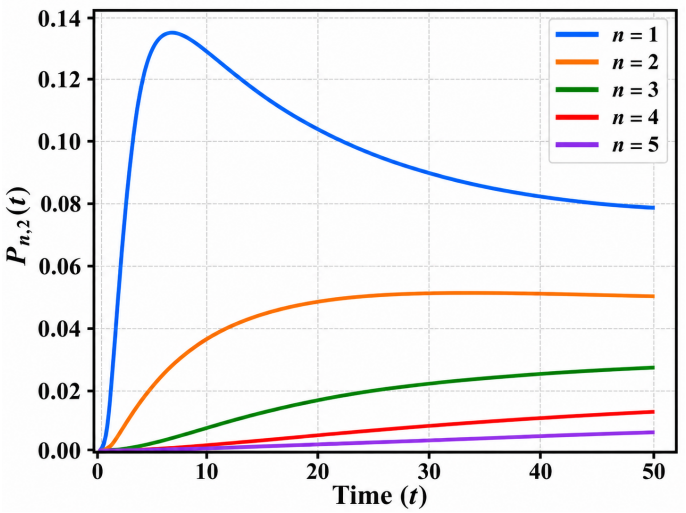


Figure 4. $P_{n,2}(t)$ versus time t.

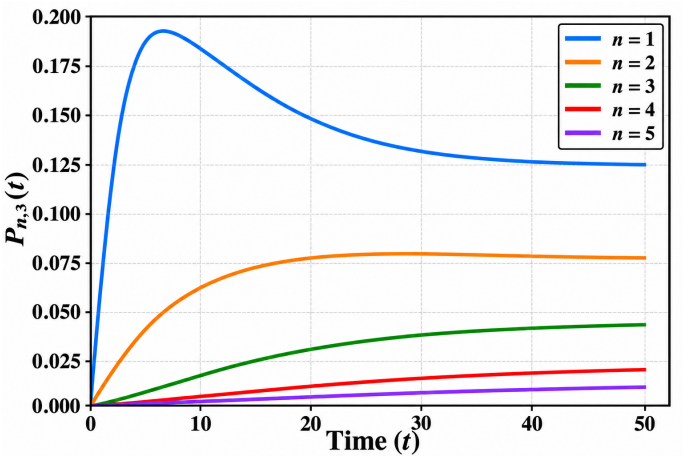


Figure 5. $P_{n,3}(t)$ versus time t.

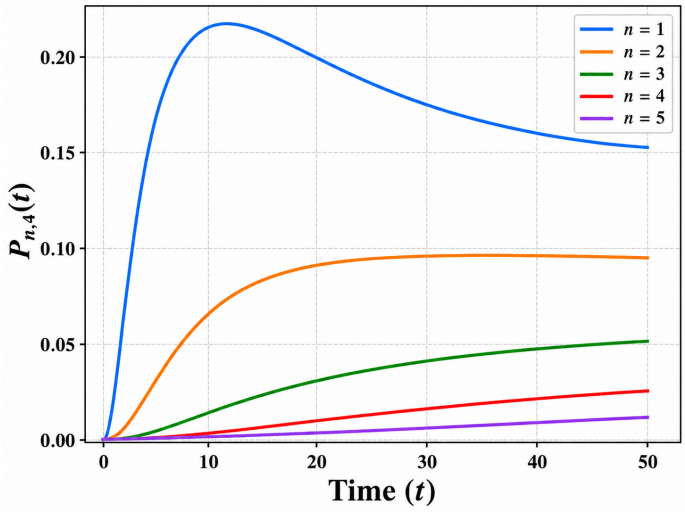


Figure 6. $P_{n,4}(t)$ versus time t.

In Figure 2–6, the mean number of packets $\mathrm{E}[N(t)]$ in the system is calculated along with phase-wise contributions. The graphical depiction provides insights into the average system load.

Table 5 summarizes the state-wise transient behaviour of the proposed multi-stage WSN model, including peak occurrence times, maximum state probabilities, and the influence of increasing packet levels.

Table 5. State-wise transient behavior of the proposed multi-stage WSN model.

State	Physical Interpretation	Peak Time for $n = 1$	Peak Probability for $n = 1$	Transient Behaviour	Effect of Increasing Level n
$j = 0$	Packet entry/ buffer state	$t = 0$	$P_{1,0}(0) = 1$	The probability starts at one, since the system initially contains one packet in the entry buffer state. It then decreases rapidly as the packet enters the sensing and communication phases.	For $n = 2$, a small peak occurs at approximately $t = 3.7$ s. For larger levels, the probabilities are small and their maxima may occur beyond the selected time horizon.

Table 5. *Cont.*

State	Physical Interpretation	Peak Time for $n = 1$	Peak Probability for $n = 1$	Transient Behaviour	Effect of Increasing Level n
$j = 1$	Active sensing state	$t \approx 1.5$ s	≈0.296	The probability increases rapidly after packet activation, reaches an early maximum, then decreases as packets move to the transmission or relay states.	Higher levels have substantially lower peak probabilities and delayed maxima. For $n \geq 3$, the probability may still be increasing at $t = 50$ s.
$j = 2$	Data transmission state	$t \approx 5.5$ s	≈0.134	The probability rises after active sensing, representing packet transmission to the next hop. Its peak occurs later than that of the sensing state.	The peak is attenuated and shifted to later times as n increases, reflecting longer queuing and forwarding delays.
$j = 3$	Relay/alternate routing state	$t \approx 8.0$ s	≈0.194	The probability exhibits a delayed and relatively broad peak, since packets may be forwarded, rerouted, or returned from adjacent communication phases.	Higher packet levels reduce the probability of occupying this state at early times and shift the relay routing activity to later times.
$j = 4$	Recovery/ interference-handling state	$t \approx 11.5$ s	≈0.221	This state has the slowest initial rise, as it is reached after the transmission and relay-related transitions. The probability has a relatively long tail due to recovery and feedback movements.	For larger n, recovery occupancy is delayed further and becomes smaller within the finite observation interval.

5.2. Variance of Packets

The variance of the number of packets $\mathrm{Var}[N(t)]$ as seen in Figure 7 serves as a crucial indicator of system predictability and stability.

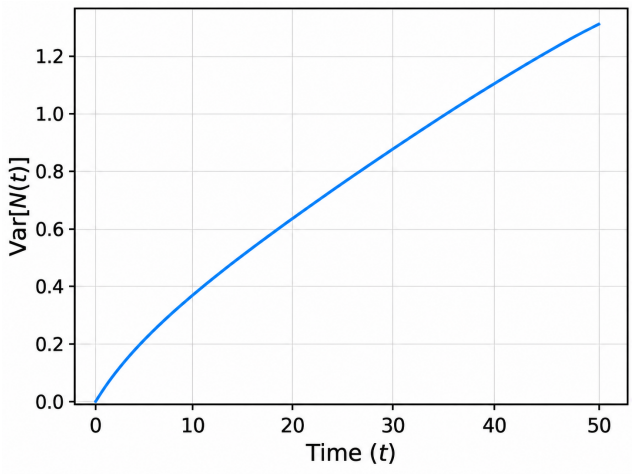


Figure 7. Variance of packets vs. time t.

The variance of the packet population is evaluated to measure fluctuations around the mean packet level. A lower variance indicates stable and predictable packet behavior in the network. A higher variance reflects large traffic fluctuations, which may cause congestion, delay, buffer overflow, and packet loss; therefore, this measure supports appropriate buffer sizing, resource allocation, and congestion control decisions. The variance complements the mean packet measure in assessing network stability and QoS performance.

Synthetic Data and Parameter Estimation

To demonstrate the proposed model's practical applicability and ease of calibration, synthetic event data were generated by simulating the CTMC event-by-event. The resulting event logs record the state transitions and corresponding holding times. These simulated observations were subsequently used to estimate selected CTMC transition rates using maximum likelihood principles. To emphasize the model's novelty and practical applicability, we generated synthetic event data by simulating the CTMC event-by-event over an extended period, thereby creating a detailed event log that mimics real-time network observations. Two key model parameters are estimated using this synthetic event log: the entry rate into phase 0, denoted λ^0, and the departure rate from phase 1 when $n \geq 2$, denoted μ_1. The estimated values were remarkably close to the 'true' values used in the simulation, showcasing how real-world data can be used to accurately calibrate the model.

Table 6 represents one stochastic sample path generated by an event-driven simulation of the proposed CTMC. Starting from the initial state $(n, j) = (1, 0)$, the admissible outgoing transitions and their corresponding rates are determined directly from the CTMC transition structure.

If $q_{(n,j),(n',j')}$ denotes the transition rate from state (n, j) to (n', j'), then the total transition rate out of the current state is given by

$$R(n, j) = \sum_{(n',j') \neq (n,j)} q_{(n,j),(n',j')}. \tag{37}$$

The state holding time Δt is generated according to an exponential distribution $\Delta t \sim \text{Exp}(R(n, j))$, and the next state (n', j') is selected with probability

$$P((n, j) \to (n', j')) = \frac{q_{(n,j),(n',j')}}{R(n, j)}. \tag{38}$$

Table 6. Sample CTMC state transitions.

Time	From n	From j	To n	To j
0.733231	1	0	1	1
3.627579	1	1	1	0
5.684994	1	0	1	1
6.562823	1	1	1	0
6.827862	1	0	1	1
6.990936	1	1	1	3
7.071799	1	3	1	1
9.005675	1	1	1	0
10.441741	1	0	1	1
11.625635	1	1	1	0

The resulting cumulative timestamps along with the state vectors before and after each event constitute the entries of Table 6. The process adheres strictly to the structural constraints $j \in \{0, 1, 2, 3, 4\}$ and $n \geq 1$; packet depletion transitions are permitted only when $n > 1$, and only transitions with strictly positive rates governed by the CTMC transition matrix are allowed.

For numerical simulation, the packet level space was truncated at $N_{\text{sim}} = 10$. Table 6 has been regenerated to replace an earlier table that reflected an unseeded Monte Carlo realization, with fixed random seeds used to ensure complete deterministic reproducibility. The corresponding implementation code and seed values are made available as well.

5.3. Overall Insights and Model Novelty

This comprehensive analysis highlights the following model capabilities:

- **Providing granular insights:** The multi-stage CTMC structure provides a detailed analysis of system behavior at each phase, offering a more nuanced understanding than simpler models.
- **Quantifying predictability:** The variance analysis directly quantifies the system's predictability, which is crucial for managing buffer sizes, preventing congestion, and ensuring QoS.
- **Supporting informed design choices:** The sensitivity analysis clearly shows the impact of various arrival rates on system stability, providing actionable intelligence with which network engineers can optimize parameters and make informed design decisions.
- **Integration with real-time data:** The demonstration of parameter estimation from event logs validates the model's capacity to be grounded in empirical data, thereby enhancing its practical utility and predictive power.

The sensitivity of packet population variance over time t for varying phase-dependent arrival rates is given in Figure 8. At $t = 100$, increasing each phase-dependent arrival rate from 0.02 to 0.08 raises packet variance $\text{Var}[N(t)]$ across all functional stages: from 2.10 to 2.88 for λ^0, 2.05 to 3.00 for λ^1, 1.98 to 3.12 for λ^2, 1.82 to 3.60 for λ^3, and 1.72 to 3.88 for λ^4. While all five curves exhibit similar increasing profiles, system sensitivity intensifies significantly in downstream phases. In particular, relay forwarding (λ^3) and recovery/re-transmission (λ^4) exert the dominant influence on packet population variability. Physically, this indicates that network congestion and queue instability compound as packets advance through the communication chain, thereby demonstrating that improving service rates and mitigating bottlenecks at relay and recovery nodes is far more critical for maintaining overall WSN stability than optimizing early-stage buffering. The sensitivity to λ^0 (the rate of new packets entering phase 0), λ^1 (the arrival rate of packets into the active sensing phase), λ^2 (the packet transmission state), λ^3 (the relay routing arrival rate), and λ^4 (the recovery phase arrival rate) also suggests that a higher rate of packets entering the above phases contributes to greater unpredictability in the system's packet count. In summary, all λ parameters ($\lambda^0, \lambda^1, \lambda^2, \lambda^3$, and λ^4) consistently show that an increase in their values leads to a higher variance in the number of packets over time. This highlights the model's ability to demonstrate how various arrival rates directly impact the predictability and stability of the system. This comprehensive sensitivity analysis is crucial for allowing network designers to understand which parameters are most influential in controlling network congestion and ensuring desired QoS.

5.4. Numerical Steady-State Evaluation

To check the QBD drift condition, we define the background phase generator

$$A = A_0 + A_1 + A_2 = \begin{bmatrix} -0.6 & 0.6 & 0 & 0 & 0 \\ 0.4 & -1 & 0.3 & 0.3 & 0 \\ 0 & 0.3 & -0.9 & 0.3 & 0.3 \\ 0 & 0.1 & 0.3 & -0.7 & 0.3 \\ 0 & 0 & 0.1 & 0.3 & -0.4 \end{bmatrix}. \tag{39}$$

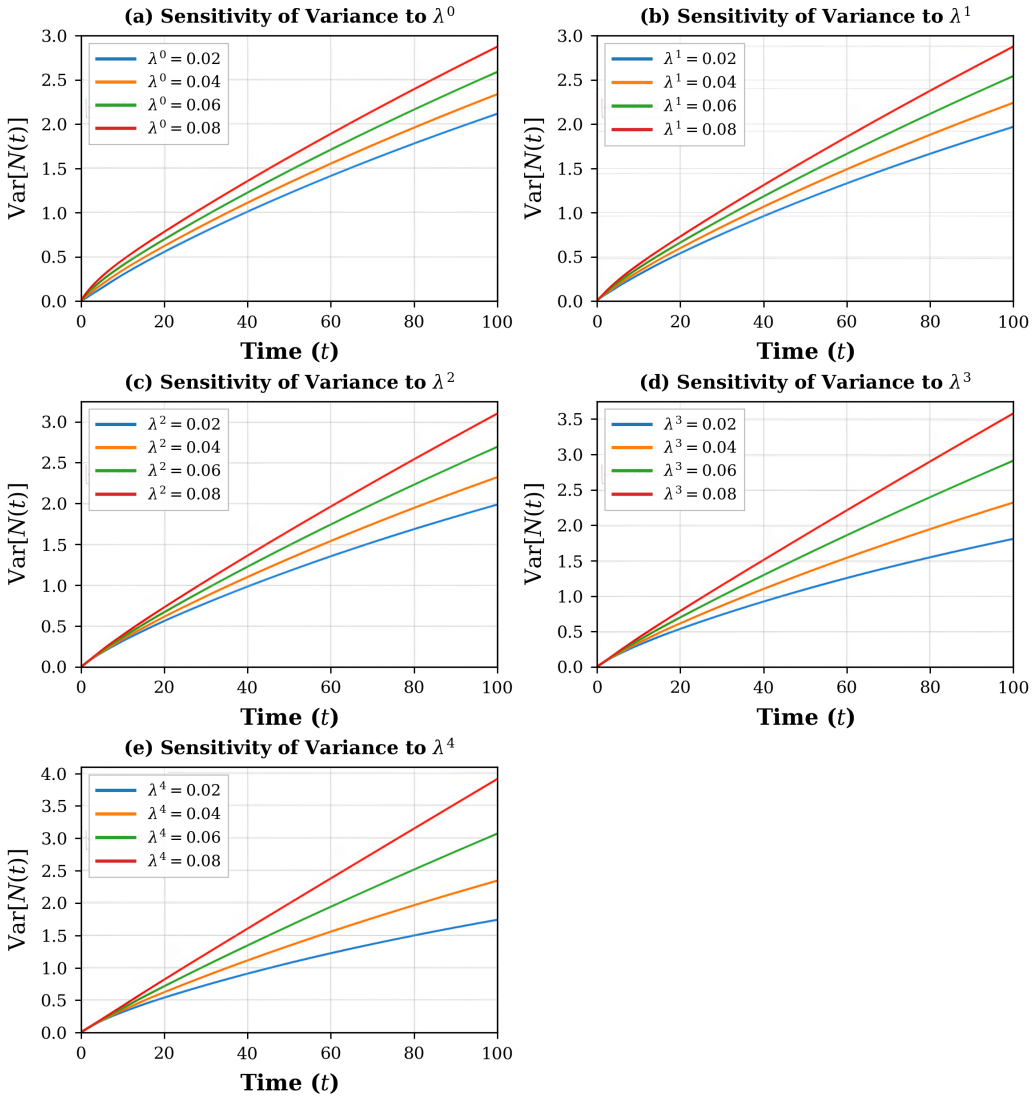


Figure 8. Sensitivity of packet population variance Var$[N(t)]$ over time t for varying phase-dependent arrival rates, showing the sensitivity of variance for (**a**) λ^0 (entry buffering phase), (**b**) λ^1 (sensing/initial processing phase), (**c**) λ^2 (wireless transmission phase), (**d**) λ^3 (relay forwarding phase), and (**e**) λ^4 (recovery/retransmission phase).

The stationary vector of this background phase process satisfies

$$\boldsymbol{\alpha} A = 0, \qquad \boldsymbol{\alpha}\mathbf{e} = 1. \tag{40}$$

Solving these equations gives

$$\boldsymbol{\alpha} = (0.0878,\ 0.1318,\ 0.1723,\ 0.2736,\ 0.3345). \tag{41}$$

The quantities α_j represent the stationary weights of the background communication phases, and are used only in evaluating the QBD drift condition. The upward and downward mean drifts are

$$d^+ = \boldsymbol{\alpha} A_0 \mathbf{e} = 0.0400$$

and

$$d^- = \boldsymbol{\alpha} A_2 \mathbf{e} = 0.0547.$$

Since

$$0.0400 < 0.0547,$$

the stability condition of the proposed QBD is satisfied.

5.5. Rate Matrix

The rate matrix R is evaluated following [20]. It is found to converge after 165 iterations, and the final R rate matrix is obtained as shown below:

$$R = \begin{bmatrix} 0.14820198 & 0.13712316 & 0.12581605 & 0.19063584 & 0.21308706 \\ 0.08736692 & 0.13978707 & 0.12576900 & 0.19000216 & 0.21110425 \\ 0.05982850 & 0.09572560 & 0.15391334 & 0.18971451 & 0.22730922 \\ 0.05479776 & 0.08767641 & 0.12261068 & 0.22609790 & 0.23027771 \\ 0.04942329 & 0.07907726 & 0.11433564 & 0.18960552 & 0.28364432 \end{bmatrix}. \quad (42)$$

6. Transition Entropy

The transition entropy is introduced as a stochastic structural measure to quantify the uncertainty in state transition of the proposed multichannel queuing system. Unlike classical performance metrics, it captures the randomness induced by environment switching and stage-dependent transitions. In many states, specifically $(n, 3)$ and $(n, 4)$, there are multiple routing choices; hence, the entropy measures play a key role in determining the uncertainty of these routing discussions, allowing for better simplicity.

If the network is stable and predictable, then a single path dominates, indicating low entropy. High entropy results if all the paths are similar, as results when the network is highly adapted and uncertain. The forward $(n+1, 3)$, backward $(n-1, 3)$, and reset $(n, 1)$ take place due to congestion. The recovery behavior analysis is obtained using the transition entropy, and is used to quantify routing uncertainty and congestion-induced randomness in the proposed model:

$$H_{\text{network}} = \sum_{(n,i)} \pi_{(n,i)} H(n, i). \quad (43)$$

The entropy-based bottleneck index is given by

$$B(n) = H(n, 3).$$

The baseline QBD uses the level-independent matrices A_0, A_1, and A_2. The transition entropy of this baseline model is computed from the embedded jump probabilities associated with the original generator $Q = [q_{ij}]$. The entropy is not computed directly from the Q matrix. The transition probabilities are obtained as $p_{ij} = \frac{q_{ij}}{-q_{ii}}, i \neq j$ for each row, where $-q_{ii} = \sum_{j \neq i} q_{ij}$.

Therefore,

$$H_{\text{system}} = \sum_{i} \pi_i H(i), \quad (44)$$

where π_i comes from the matrix-geometric solution. We find that the large rates $(0.3, 0.3)$ dominate. The probabilities become almost equal $(0.47, 0.47)$, indicating high uncertainty in routing, i.e., high entropy. This indicates the presence of strong parallel transitions (relay plus recovery).

The entropy analysis indicates that stochastic variability is primarily induced during packet forwarding. The entropy analysis presented in Table 7 and Figure 9 indicates that transition uncertainty is highest in the data-transmission state (1.349 bits), followed by the sensing state (1.335 bits), whereas the relay-forwarding and recovery states exhibit comparatively lower entropy values of 1.264 and 1.000 bits, respectively. The entropy remains invariant across the levels, indicating that the routing uncertainty is the same throughout the network. Therefore, the network is analyzed by making the parameter depend on the level of transition n.

Table 7. Entropy values.

State	Entropy (Bits)
$(n,1)$	1.335
$(n,2)$	1.349
$(n,3)$	1.264
$(n,4)$	1.000

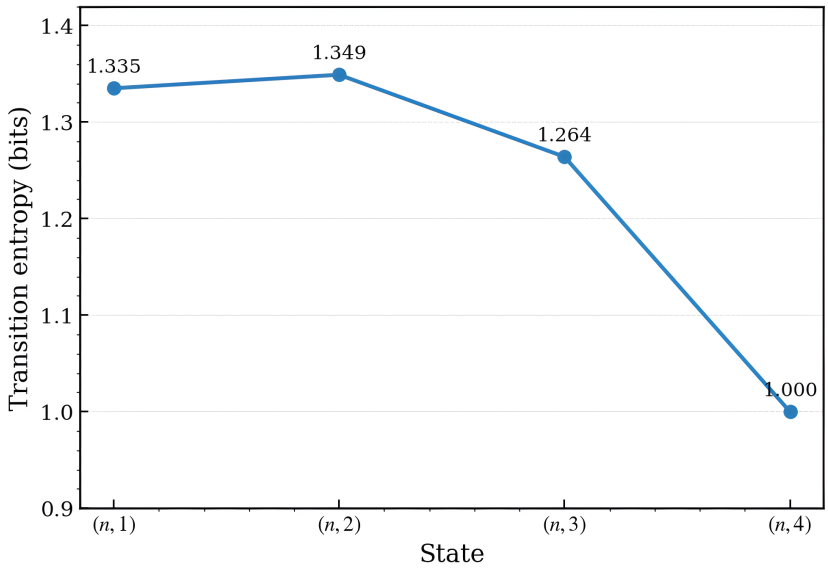


Figure 9. Average number of packets at t (entropy vs. state).

We impose the following restrictions: congestion increase with level

$$\delta_B(n) = 0.3 + 0.02n,$$

and service decreases with level

$$\mu(n) = 0.06 - 0.002n.$$

This results in a change in the entropy with variation in n.

Now, varying δ_B from 0.1 to 0.5 and plotting $H(n,3)$ vs. δ_B gives a strong performance curve, as seen in Figures 10 and 11. From above two graphs, it can be observed that the entropy associated with the relay state $H(n,3)$ decreases significantly as the level n increases. Thus, the routing decision becomes more deterministic under higher congestion. This leads to reduced flexibility of packet movement.

The sensing state $H(n,1)$ remains nearly constant across all levels, showing stable system behavior that is unaffected by congestion. The gradual decline in entropy noticed in the transition state $H(n,2)$ depicts moderate uncertainty. The recovery state $H(n,4)$ follows a structured transition pattern independent of network load, and remains constant. These results highlight that the relay states act as critical points of congestion where the system transitions from stochastic to deterministic behavior.

Extension: Level-Dependent Transition Entropy

This extension is not used to compute the baseline transient probabilities $P_{n,j}(t)$, the baseline stability condition, or the constant rate matrix R. In a genuinely level-dependent version of the model, a single homogeneous relation $\pi_i = \pi_1 R^{n-1}$ is not generally applicable; a level-dependent matrix-analytic formulation would be required.

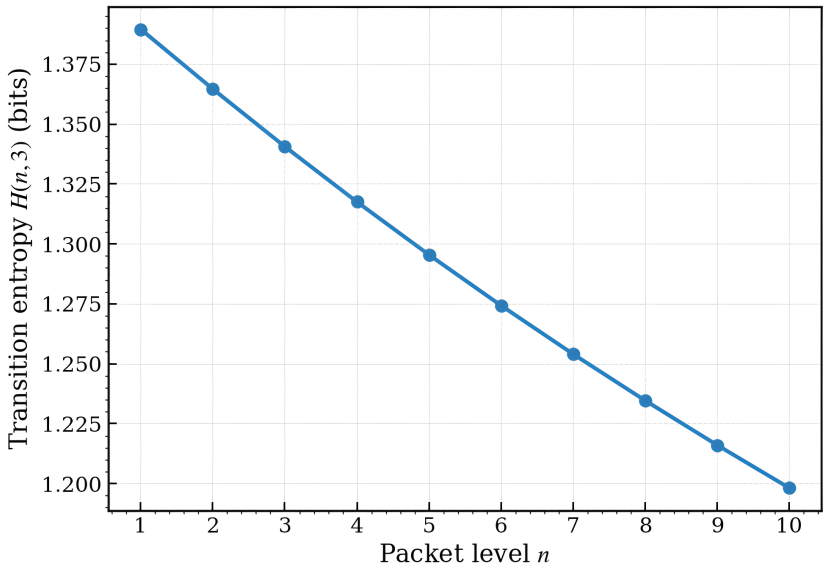


Figure 10. Average number of packets at t ($H(n,3)$ vs. level n).

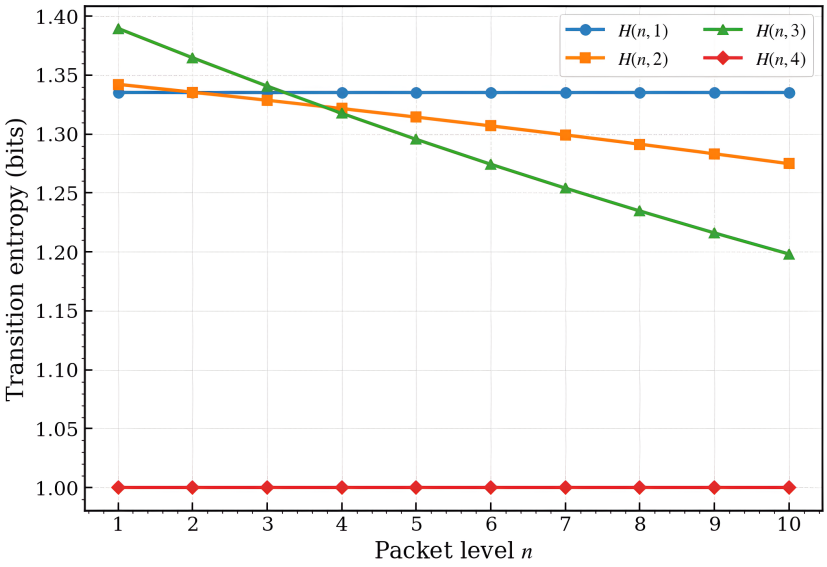


Figure 11. Average number of packets at t (entropy vs. level n).

7. WSN Model of the Proposed Grid

The mathematical model and numerical solution may be thought of as representing a fragment of a large WSN as shown in Figure 12. A system of differential equations is developed to model transitions between different states. These transitions capture the packet movement and node interaction. In this way, the model helps us to investigate the dynamic system behaviors fundamental to WSNs. We employ a Markov chain model for predictive node connectivity and failure recovery. Parameters such as δ_B, δ_{DB}, p, and q govern the network delay and reliability, as in the protocols from [38].

Numerical Results Using Monte Carlo Simulation

Figures 13 and 14 together with Table 8 validate the proposed CTMC representation of the considered WSN fragment.

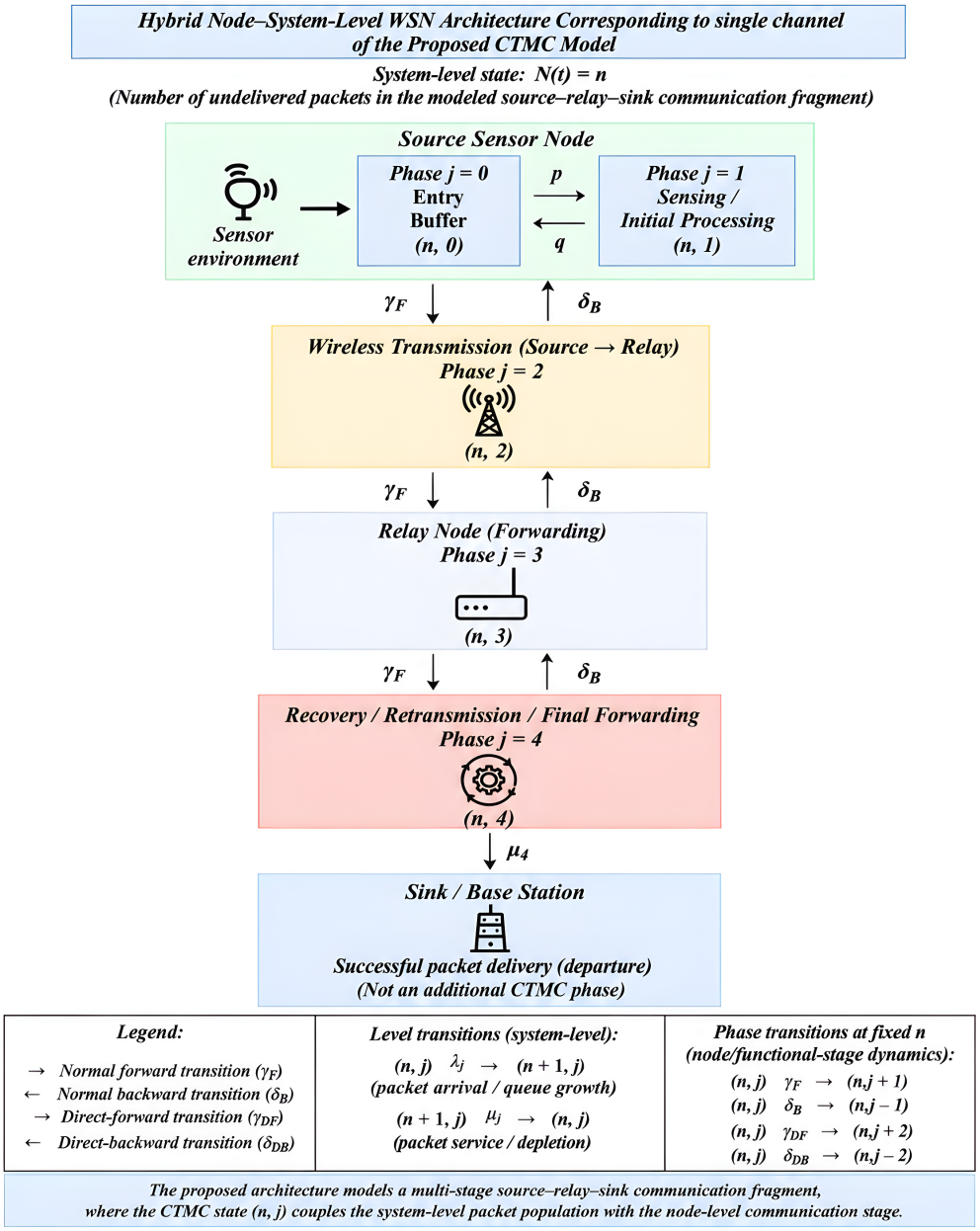


Figure 12. Proposed packet movement and node interaction grid.

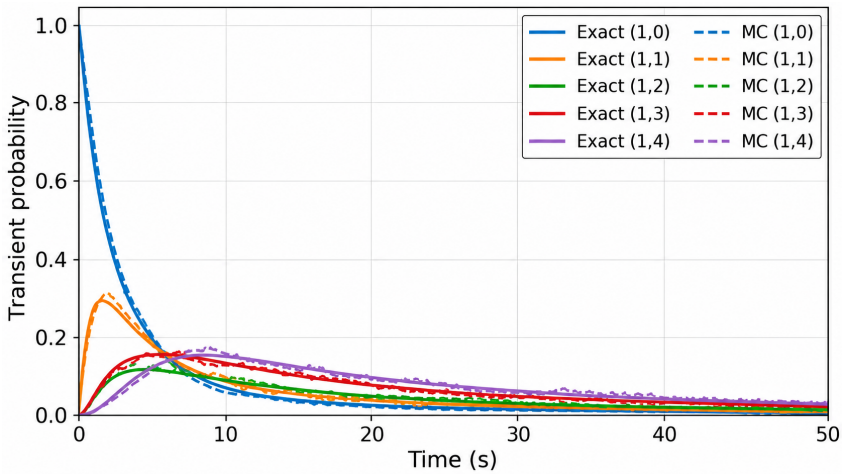


Figure 13. Transient probability validation for State 1.

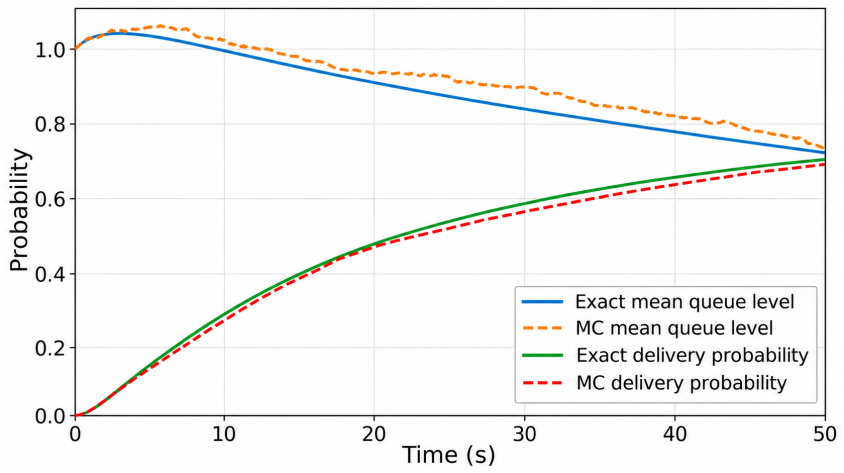


Figure 14. Queue evolution and delivery probability.

Table 8. Performance summary.

Performance Measure	Monte Carlo	Exact CTMC
Packet delivery probability	0.6875	0.7017
Overflow probability	0.0035	0.0033
Mean queue level at $t = 50$ s	0.7370	0.7219
Mean delay conditional on delivery (s)	16.7221	–
Mean time to overflow (s)	41.5680	–

Figure 13 compares the analytical and Monte Carlo transient probabilities for the five packet processing phases at level $(i = 1)$. Because the system initially starts in the entry state $(1, 0)$, the probability $P_{1,0}(t)$ decreases rapidly as packets progress through the active sensing, transmission, relay routing, and recovery phases. The probability of state $(1, 1)$ reaches an early peak, whereas the probabilities of $(1, 2)$, $(1, 3)$, and $(1, 4)$ increase more gradually, reflecting the sequential processing, forwarding, rerouting, and recovery of packets in the WSN fragment. The close correspondence between the exact and Monte Carlo curves confirms that the simulation accurately reproduces the transient behavior of the proposed CTMC.

Figure 14 presents the corresponding aggregate performance measures. The mean queue level initially increases slightly because of short-term packet accumulation in the entry and intermediate communication phases, then subsequently decreases as packets are forwarded and successfully cleared from the network. In contrast, the cumulative packet delivery probability increases monotonically with time and reaches approximately 0.70 at $t = 50$ s. This complementary behavior indicates that the reduction in packet backlog is associated with successful packet delivery to the sink.

Table 8 provides numerical confirmation of these observations. The calculations are carried out using Python code with 2000 replications and a simulation horizon of 50 s. The mean absolute error for $P_{1,j}(t)$, $j = 0$ to 4 is 0.0036. The Monte Carlo estimates closely match the analytical results for delivery probability, overflow probability, and mean queue level.

In particular, the exact and simulated delivery probabilities are (0.7017) and (0.6875), respectively, while the corresponding overflow probabilities remain below (0.004), indicating that buffer overflow is rare for the selected parameter set. The mean absolute error (0.0036) for the level-one transient probabilities further demonstrates close agreement between the analytical solution and the simulation-based estimates.

Overall, these results support the suitability of the proposed CTMC as a stochastic representation of packet movement, relay forwarding, recovery, and congestion evolution in the considered WSN communication fragment.

8. Comparison with Existing Studies

Table 9 presents a comparative summary of representative studies and the proposed model, highlighting differences in modeling approaches, analytical techniques, and performance measures. The comparison emphasizes the distinctive contribution of the proposed hybrid node–system-level CTMC/QBD framework, integrating multi-stage packet processing, dynamic routing, and transient and steady-state analyses.

Table 9. Summary and comparison of representative studies with the proposed model.

Reference/Year	Methodology and Focus	Key Finding	Limitation Relative to Present Work
Yenugula [1], 2024	Markov-chain optimization with enhanced TDMA–CSMA for QoS, energy efficiency and reliable communication.	Improves communication reliability through adaptive slot and collision-control mechanisms.	Protocol-oriented; does not jointly model packet population and multistage communication phases using a CTMC/QBD.
Deepakraj and Raja [2], 2021	Markov-chain-based energy-aware routing using node location and residual energy.	Evaluates routing using energy consumption, delay and residual-energy measures.	Routing-oriented; does not provide coupled transient and steady-state packet-stage analysis.
Khujamatov et al. [3], 2020	Markov chain modeling of ZigBee bandwidth states and IEEE 802.15.4 CSMA/CA.	Examines transmission probability, interference, and bandwidth state behavior.	MAC-layer model; does not jointly represent sensing, transmission, relay, and recovery stages.
Ma et al. [4], 2025	Stackelberg game and Lyapunov optimization for traffic offloading and end-to-end reliability.	Improves traffic scheduling, delay, and transmission reliability.	Optimization framework; does not derive stage-wise CTMC transient probabilities.
Jayamani et al. [5], 2024	N-policy $M/M/1$ queue for network energy saving.	Studies energy consumption, queue length, idle periods, and operational cost.	Single-server model; does not include the five communication stages and relay/recovery transitions.
Villordo-Jimenez et al. [7], 2024	Distance-based queuing for relay scheduling in linear WSNs.	Improves packet loss uniformity, throughput, reliability, and scalability.	Distance-priority model; does not use a joint five-stage CTMC/QBD representation.
Kumar et al. [14], 2009	Multi-server feedback retrial QBD with finite waiting capacity.	Derives stability and performance measures using the matrix-geometric method.	General retrial queue; no architecture-correlated WSN packet-stage interpretation.
Blondia [22], 2021	Finite-capacity queue with repeated vacations for an energy harvesting WSN node.	Derives occupancy and waiting time characteristics.	Energy/sleep focused; does not couple packet population with communication-stage dynamics.

Table 9. *Cont.*

Reference/Year	Methodology and Focus	Key Finding	Limitation Relative to Present Work
Kempa and Kurzyk [23], 2022	Threshold power-saving queue with Laplace transform transient analysis.	Obtains a Laplace representation of transient queue size probabilities.	Power-saving model; does not integrate relay, recovery, and QBD steady-state analysis.
Zhang et al. [28], 2023	Adaptive N-policy $M/M/1/C$ queue for sleep scheduling and reliability.	Evaluates packet delay and timely reliability.	Power management model; does not explicitly include relay, rerouting, and recovery phases.
Shudrenko and Timm-Giel [30], 2024	Queuing and combinatorial analysis for end-to-end delay in TSCH WSNs.	Provides analytical estimation of communication latency.	Delay-focused; does not jointly analyze packet-level transient, steady-state, and recovery dynamics.
Kumar et al. [31], 2024	Continuous-time Markov process for WSN reliability and sensitivity analysis.	Shows how transition rate variations affect network reliability.	Reliability-focused; does not couple packet population with five communication stages.
Singh et al. [32], 2026	DTMC transient analysis with hybrid spectrum access, sleep modes, and multi-objective optimization.	Studies energy efficiency, imperfect sensing, and spectrum-access decisions.	Cognitive radio model; does not provide architecture-correlated WSN packet-stage QBD coupling.
Champati et al. [33], 2020	Stochastic network calculus for multi-hop wireless networks under static routing.	Derives transient end-to-end delay and backlog bounds.	Provides network-level bounds rather than explicit internal communication-stage probabilities.
Sudhesh and Mohammed Shapique [34], 2022	Multiple vacation queue with threshold policy for WSN power management.	Provides transient and steady-state measures for busy, wake-up, shutdown, and inactive modes.	States represent power management modes rather than packet processing and communication stages.
Present work	Multi-stage CTMC/QBD coupling packet level with buffering, sensing, transmission, relay forwarding, and recovery phases.	Provides transient and steady-state probabilities, stability, mean/variance, entropy, sensitivity, and parameter estimation.	Couples the undelivered packet level $N(t)$ with the five-stage communication process $E(t)$ in one architecture-correlated framework.

9. List of Abbreviations

The abbreviations and acronyms used throughout the manuscript are summarized in Table 10 to provide a clear understanding of the mathematical notation and technical terminology. This table serves as a reference for the key concepts and analytical methods employed in the proposed multi-stage WSN model.

Table 10. List of abbreviations used in the manuscript.

Abbreviation	Full Form
AODV	Ad Hoc On-Demand Distance Vector
CSMA	Carrier Sense Multiple Access

Table 10. *Cont.*

Abbreviation	Full Form
CSMA/CA	Carrier Sense Multiple Access with Collision Avoidance
CTMC	Continuous-Time Markov Chain
DSDV	Destination-Sequenced Distance Vector
IoT	Internet of Things
LEACH	Low-Energy Adaptive Clustering Hierarchy
MAC	Medium Access Control
MLE	Maximum Likelihood Estimation
QBD	Quasi-Birth-and-Death
QoS	Quality of Service
SDN	Software-Defined Networking
TDMA	Time-Division Multiple Access
TSCH	Time-Slotted Channel Hopping
WMN	Wireless Mesh Network
WSN	Wireless Sensor Network

10. Conclusions

This study presents a multi-stage Markov chain model for analyzing both steady-state and transient behaviors in wireless sensor networks (WSNs). By mathematically modeling packet movement, congestion handling, and recovery mechanisms, the proposed framework provides valuable insights into network retransmission dynamics and system efficiency.

The analysis of transition entropy reveals critical insights into system instability and congestion patterns across different states. The analytical derivations and numerical simulations illustrate how state transitions influence packet flow, thereby enabling optimized routing and enhanced connectivity in large-scale WSN deployments. The numerical results reveal phase-dependent transient behavior and show that packet count variance is an effective indicator of network stability, congestion risk, and QoS performance. Moreover, sensitivity and synthetic data analyses confirm that the model can support arrival rate control, buffer design, and practical parameter calibration. Finally, a WSN model is fitted for network and numerical validation carried out using the Monte Carlo method. In future work, these equations could be extended into adaptive priority queue-based models found in wireless mesh networks (WMN) and software-defined networking (SDN). It would also be possible to model real-world implementations using AODV, DSDV, or LEACH protocols, which rely on transient-state analysis for efficient routing. In addition to queuing delay, propagation delay and processing delay could also be incorporated, which would make the model more appropriate for real-time networks.

Author Contributions: Conceptualization, H.K., L.G. and S.A.; methodology, H.K. and A.N.; software, L.G., A.N. and S.A.; validation, A.N., S.A. and B.S.; formal analysis, H.K., L.G., A.N. and S.A.; investigation, B.S.; resources, B.S.; data curation, L.G., A.N. and S.A.; writing—original draft, H.K.; writing—review and editing, B.S.; visualization, L.G., A.N. and S.A.; project administration, L.G., A.N. and B.S.; funding acquisition, B.S. All authors have read and agreed to the published version of the manuscript.

Funding: The present research was conducted with a 2026 research grant from Kwangwoon University.

Data Availability Statement: The original contributions presented in this study are included in the article. Further inquiries can be directed to the corresponding authors.

Acknowledgments: This work was supported by Kwangwoon University, Seoul, Republic of Korea. The authors declare that they did not use generative AI or AI-assisted technologies in the writing of this manuscript.

Conflicts of Interest: The authors declare no conflict of interest.

Appendix A. Supporting Derivations of the Laplace–Generating Function–Bessel Transient Representation

This appendix provides the supplementary mathematical derivations associated with the transient solution of the proposed five-phase CTMC/QBD model. The generating function approach, Laplace transform formulation, and modified Bessel function representation are presented here to avoid overloading the main body of the manuscript with standard analytical steps.

Appendix A.1. Generating Function Formulation

Let

$$P_{n,j}(t) = P\{N(t) = n, E(t) = j\}, \qquad n \geq 1, \quad j = 0, 1, 2, 3, 4$$

denote the transient probability of the system containing n undelivered packets and being in communication phase j at time t.

For each phase j, define the probability generating function

$$G_j(z,t) = \sum_{n=1}^{\infty} P_{n,j}(t) z^n, \qquad j = 0, 1, 2, 3, 4. \tag{A1}$$

Multiplying the corresponding transient balance equations by z^n and summing over $n \geq 1$ converts the level-dependent differential equations into equations involving $G_j(z,t)$. In particular, the level-increasing and level-decreasing terms generate factors proportional to z and z^{-1}, respectively.

For phases $j = 1, 2, 3, 4$, the resulting generating function equation can be written in the general form

$$\frac{\partial G_j(z,t)}{\partial t} = -\left[k_j - \lambda^j z - \frac{\mu_j}{z}\right] G_j(z,t) + F_j(z,t), \tag{A2}$$

where k_j denotes the total rate leaving phase j, while $F_j(z,t)$ collects the inflow contributions from the remaining communication phases and boundary terms.

Appendix A.2. Laplace Transform Treatment of the Entry Buffer State

For the entry buffer phase $j = 0$, the transient probability satisfies the corresponding balance relation. The Laplace transform of $P_{n,0}(t)$ is defined as

$$\widetilde{P}_{n,0}(s) = \int_0^{\infty} e^{-st} P_{n,0}(t)\, dt. \tag{A3}$$

The initial condition used throughout the transient analysis is

$$P_{1,0}(0) = 1, \qquad P_{n,0}(0) = 0, \quad n > 1, \tag{A4}$$

with all other phase probabilities initially equal to zero.

Applying the Laplace transform to the differential equation for the entry buffer state gives

$$s\widetilde{P}_{n,0}(s) - P_{n,0}(0) = \mathcal{L}\left\{\frac{dP_{n,0}(t)}{dt}\right\}, \tag{A5}$$

which leads to an algebraic representation for $\widetilde{P}_{n,0}(s)$. The corresponding time-domain probability $P_{n,0}(t)$ is obtained by inverse Laplace transformation.

The resulting $P_{n,0}(t)$ subsequently contributes to the coupled equations associated with the remaining phases.

Appendix A.3. Modified Bessel Function Expansion

To obtain the state probabilities from the generating function representation, define

$$\alpha_j = 2\sqrt{\lambda^j \mu_j}, \qquad \beta_j = \sqrt{\frac{\lambda^j}{\mu_j}}, \qquad j = 1, 2, 3, 4. \tag{A6}$$

Using the generating identity for the modified Bessel function of the first kind,

$$\exp\left[\frac{x}{2}\left(w + \frac{1}{w}\right)\right] = \sum_{r=-\infty}^{\infty} I_r(x) w^r, \tag{A7}$$

and the level-transition kernel can be expanded in terms of $I_r(\cdot)$.

For the lower-bounded packet level $n \geq 1$, the corresponding kernel may be written as

$$K_j(n, m, \tau) = \beta_j^{n-m}\left[I_{n-m}(\alpha_j \tau) - I_{n+m}(\alpha_j \tau)\right] e^{-k_j \tau}, \tag{A8}$$

where $\tau = t - u$. Here, $I_r(\cdot)$ denotes the modified Bessel function of the first kind of order r, the first term $I_{n-m}(\alpha_j \tau)$ describes level propagation between packet states, and the second term $I_{n+m}(\alpha_j \tau)$ accounts for the lower-boundary correction associated with the restriction $n \geq 1$.

The factor β_j^{n-m} captures the imbalance between the upward rate λ^j and the downward rate μ_j, while $e^{-k_j \tau}$ represents attenuation due to the total rate of leaving phase j.

Appendix A.4. Coupled Integral Representation

The Bessel representation does not decouple the communication phases. The probabilities remain mutually dependent through the phase transition terms contained in the forcing function F_j.

Accordingly, the transient probability for phase j may be expressed in the general form

$$P_{n,j}(t) = \sum_{m=1}^{\infty} K_j(n, m, t) P_{m,j}(0) + \int_0^t \sum_{m=1}^{\infty} K_j(n, m, t - u) F_{m,j}(u)\, du, \tag{A9}$$

where $F_{m,j}(u)$ represents the total inflow into state (m, j) from the other communication phases.

Appendix B. Supporting QBD Theory and Computational Derivations

Appendix B.1. Details of the Q Matrix

Structure of the blocks of the Q matrix For completeness and reproducibility, the explicit forms of the QBD block matrices B_0, A_0, A_1, and A_2 are provided together with their corresponding diagonal elements.

$$B_0 = \begin{bmatrix} \theta_1^0 & p & 0 & 0 & 0 \\ q & \theta_2^0 & \gamma_F & \gamma_{DF} & 0 \\ 0 & \delta_B & \theta_3^0 & \gamma_F & \gamma_{DF} \\ 0 & \delta_{DB} & \delta_B & \theta_4^0 & \gamma_F \\ 0 & 0 & \delta_{DB} & \delta_B & \theta_5^0 \end{bmatrix}, \tag{A10}$$

$$A_0 = \begin{bmatrix} \lambda^0 & 0 & 0 & 0 & 0 \\ 0 & \lambda^1 & 0 & 0 & 0 \\ 0 & 0 & \lambda^2 & 0 & 0 \\ 0 & 0 & 0 & \lambda^3 & 0 \\ 0 & 0 & 0 & 0 & \lambda^4 \end{bmatrix}, \tag{A11}$$

$$A_1 = \begin{bmatrix} \theta_1^* & p & 0 & 0 & 0 \\ q & \theta_2^* & \gamma_F & \gamma_{DF} & 0 \\ 0 & \delta_B & \theta_3^* & \gamma_F & \gamma_{DF} \\ 0 & \delta_{DB} & \delta_B & \theta_4^* & \gamma_F \\ 0 & 0 & \delta_{DB} & \delta_B & \theta_5^* \end{bmatrix}, \tag{A12}$$

and

$$A_2 = \begin{bmatrix} 0 & 0 & 0 & 0 & 0 \\ 0 & \mu_1 & 0 & 0 & 0 \\ 0 & 0 & \mu_2 & 0 & 0 \\ 0 & 0 & 0 & \mu_3 & 0 \\ 0 & 0 & 0 & 0 & \mu_4 \end{bmatrix}. \tag{A13}$$

The diagonal elements of B_0 are defined by

$$\begin{aligned} \theta_1^0 &= -(p + \lambda^0), \\ \theta_2^0 &= -(q + \gamma_F + \gamma_{DF} + \lambda^1), \\ \theta_3^0 &= -(\delta_B + \gamma_F + \gamma_{DF} + \lambda^2), \\ \theta_4^0 &= -(\delta_{DB} + \delta_B + \gamma_F + \lambda^3), \\ \theta_5^0 &= -(\delta_{DB} + \delta_B + \lambda^4). \end{aligned} \tag{A14}$$

Similarly, the diagonal elements of A_1 are given by

$$\begin{aligned} \theta_1^* &= -(p + \lambda^0), \\ \theta_2^* &= -(\mu_1 + q + \gamma_F + \gamma_{DF} + \lambda^1), \\ \theta_3^* &= -(\mu_2 + \delta_B + \gamma_F + \gamma_{DF} + \lambda^2), \\ \theta_4^* &= -(\mu_3 + \delta_{DB} + \delta_B + \gamma_F + \lambda^3), \\ \theta_5^* &= -(\mu_4 + \delta_{DB} + \delta_B + \lambda^4). \end{aligned} \tag{A15}$$

Clearly,

$$A_0 + RA_1 + R^2A_2 = 0.$$

Appendix B.2. Computational Algorithm for the Complete Transient Probability Vector

The Laplace–matrix-Bessel formulation characterizes the analytical propagation structure of the coupled transient system. Since the individual phase probabilities remain coupled through the entry buffer forcing, feedback transitions, and boundary at $n = 1$, the complete transient probability vector is evaluated numerically through the equivalent truncated continuous-time Markov chain (CTMC) generator. The computational procedure used to obtain the reported transient probabilities is presented below.

Algorithmic Computation of the Complete Transient Probability Vector

Input: The transition rates p, q, γ_F, γ_{DF}, δ_B, δ_{DB}, λ^j for $j = 0, 1, 2, 3, 4$, and μ_j for $j = 1, 2, 3, 4$; the truncation level $N_{\max}$; the final observation time T; and the time grid $0 = t_0 < t_1 < \cdots < t_K = T$.

Initial condition:

$$X(0) = (1, 0),$$

or equivalently,

$$P_{1,0}(0) = 1,$$

with all remaining state probabilities equal to zero.

Output: The complete transient probability vector $\mathbf{\Pi}^{(N)}(t_k)$ and the individual transient probabilities

$$P_{n,j}(t_k), \qquad 1 \le n \le N_{\max}, \qquad j \in \{0, 1, 2, 3, 4\}.$$

Step 1. Define the truncated state space.

For numerical computation, truncate the infinite packet-level space at $N_{\max}$ and define $\mathcal{S}_N = \{(n, j) : 1 \le n \le N_{\max}, j \in \{0, 1, 2, 3, 4\}\}$. Each state (n, j) is assigned the matrix index

$s(n,j) = 5(n-1)+j$. Therefore, the total number of states in the truncated CTMC is $5N_{\max}$, and the corresponding finite generator has dimension $5N_{\max} \times 5N_{\max}$.

Step 2. Construct the within-level phase transition matrix.

$$C = \begin{pmatrix} -p & p & 0 & 0 & 0 \\ q & -(q+\gamma_F+\gamma_{DF}) & \gamma_F & \gamma_{DF} & 0 \\ 0 & \delta_B & -(\delta_B+\gamma_F+\gamma_{DF}) & \gamma_F & \gamma_{DF} \\ 0 & \delta_{DB} & \delta_B & -(\delta_{DB}+\delta_B+\gamma_F) & \gamma_F \\ 0 & 0 & \delta_{DB} & \delta_B & -(\delta_{DB}+\delta_B) \end{pmatrix} \tag{A16}$$

Its diagonal entries are obtained from $C_{jj} = -\sum_{k\neq j} C_{jk}$, so that $C\mathbf{e} = \mathbf{0}$, where $\mathbf{e}$ denotes the column vector of ones.

Step 3. Construct the QBD block matrices.

The upward level-transition block, corresponding to an increase in the number of undelivered packets, is

$$A_0 = \mathrm{diag}\left(\lambda^0, \lambda^1, \lambda^2, \lambda^3, \lambda^4\right).$$

The downward level-transition block is

$$A_2 = \mathrm{diag}(0, \mu_1, \mu_2, \mu_3, \mu_4).$$

The zero in the first diagonal position reflects the fact that the entry-buffer phase does not have a packet depletion transition. For the interior levels $n \geq 2$, define

$$A_1 = C - \mathrm{diag}\left(\lambda^0, \lambda^1+\mu_1, \lambda^2+\mu_2, \lambda^3+\mu_3, \lambda^4+\mu_4\right).$$

At the lower boundary $n = 1$, packet depletion transitions below level one are not permitted; hence, define

$$B_0 = C - diag\left(\lambda^0, \lambda^1, \lambda^2, \lambda^3, \lambda^4\right).$$

Thus,

$$B_0 = A_1 + A_2.$$

Step 4. Establish the Laplace–matrix-Bessel representation.

For the entry buffer phase $j = 0$, define the generating function

$$P(z,t) = \sum_{n=1}^{\infty} P_{n,0}(t) z^n$$

and

$$F_1(z,t) = \sum_{n=1}^{\infty} P_{n,1}(t) z^n.$$

Taking the Laplace transform gives

$$\widetilde{P}(z,s) = \frac{z + q\tilde{F}_1(z,s)}{s + p + \lambda^0 - \lambda^0 z}.$$

For the four operational phases $j = 1, 2, 3, 4$, define

$$\mathbf{u}_n(t) = \left[P_{n,1}(t), P_{n,2}(t), P_{n,3}(t), P_{n,4}(t)\right].$$

For homogeneous upward and downward level transition rates, the scalar modified Bessel propagation kernel is $b_r(t) = e^{-(\lambda+\mu)t}\left(\frac{\lambda}{\mu}\right)^{r/2} I_r\left(2t\sqrt{\lambda\mu}\right)$, where $I_r(\cdot)$ denotes the modified Bessel function of the first kind of order r. The corresponding matrix–Bessel kernel is $K_r(t) = b_r(t)e^{C_4 t}$, where C_4 is the within-level phase transition matrix associated with

phases $j = 1, 2, 3, 4$. The Laplace relation and matrix–Bessel kernel characterize the analytical propagation structure of the transient system; however, the complete transient probabilities cannot be evaluated independently because the entry buffer phase, the four operational phases, the feedback transitions, and the boundary at $n = 1$ all remain coupled. Therefore, the complete coupled probability vector is evaluated simultaneously using the finite CTMC generator.

Step 5. Construct the finite CTMC generator.

For a truncation level $N_{\max}$, construct Q_N. For the blocked arrival treatment at the upper numerical boundary, $A_1^{(N)}$. Consequently,

$$A_2\mathbf{e} + A_1^{(N)}\mathbf{e} = A_2\mathbf{e} + (A_1 + A_0)\mathbf{e} = \mathbf{0}.$$

Thus, the upper-boundary row of the truncated generator remains conservative.

Step 6. Check the generator consistency.

Verify that every off-diagonal element satisfies $(Q_N)_{rs} \geq 0 r \neq s$ and that every row of the generator sums to zero: $Q_N\mathbf{e} = \mathbf{0}$.

The numerical row-sum error is computed as

$$\varepsilon_Q = \max_r \left| \sum_s (Q_N)_{rs} \right|.$$

The generator is accepted when ε_Q is within machine precision and all off-diagonal transition rates are non-negative.

Step 7. Form the initial probability vector.

The system initially contains one packet in the entry-buffer phase; therefore, $P_{1,0}(0) = 1$ and $P_{n,j}(0) = 0$ for all remaining states. Hence, the finite initial probability vector is $\Pi^{(N)}(0) = (1, 0, 0, 0, 0, 0, \ldots, 0)$.

Step 8. Compute the complete transient probability vector.

For each required time instant $t_k, k = 0, 1, \ldots, K$, evaluate $\mathbf{\Pi}^{(N)}(t_k) = \mathbf{\Pi}^{(N)}(0)e^{Q_N t_k}$. Equivalently, if the probability vector is represented as a column vector, the numerical computation is $\boxed{\mathbf{p}(t_k) = e^{Q_N^T t_k}\mathbf{p}(0)}$.

Step 9. Extract the individual state probabilities.

For each $n = 1, 2, \ldots, N_{\max}$ and $j = 0, 1, 2, 3, 4$, extract the state probability according to

$$P_{n,j}(t_k) = \left[\mathbf{\Pi}^{(N)}(t_k)\right]_{s(n,j)}.$$

Using the indexing rule

$$s(n, j) = 5(n - 1) + j,$$

the complete probability vector can be rearranged as

$$\mathbf{\Pi}^{(N)}(t) = \left[P_{1,0}(t), P_{1,1}(t), \ldots, P_{1,4}(t), P_{2,0}(t), \ldots, P_{N_{\max},4}(t)\right].$$

The probabilities $P_{n,j}(t)$ are not evaluated independently; they are components of the complete coupled transient solution.

Step 10. Verify probability normalization.

For each time instant t_k, calculate

$$S(t_k) = \sum_{n=1}^{N_{\max}} \sum_{j=0}^{4} P_{n,j}(t_k).$$

The normalization error is

$$\varepsilon_{\text{prob}} = \max_{0\le k\le K} |S(t_k) - 1|.$$

The transient calculation is accepted when $\varepsilon_{\text{prob}}$ is within the prescribed numerical tolerance.

Step 11. Verify truncation convergence.

Because the original QBD has an infinite packet-level space, repeat the transient computation for increasing truncation levels, for example, $N_{\max} = 40,\ 60,\ 80,\ 100$. For two truncation levels $N_a < N_b$, calculate

$$D(N_a, N_b) = \max_{\substack{0\le t\le T\\ 1\le n\le 5\\ 0\le j\le 4}} \left| P_{n,j}^{(N_a)}(t) - P_{n,j}^{(N_b)}(t) \right|.$$

The truncation is considered sufficient when $D(N_a, N_b) < \varepsilon_{\text{trunc}}$ and the probability mass at the upper boundary $\sum_{j=0}^{4} P_{N_{\max},j}(t)$ is negligible throughout the observation interval. For the numerical implementation used in this study, the truncation level is selected as $N_{\max} = 80$.

Step 12. Compute the transient performance measures.

The mean number of packets is calculated as

$$E[N(t)] = \sum_{n=1}^{N_{\max}} \sum_{j=0}^{4} n P_{n,j}(t).$$

Therefore, the final numerical outputs are $\left\{P_{n,j}(t_k)\right\}, E[N(t_k)], \text{Var}[N(t_k)]$ for $n = 1, \dots, N_{\max}, j = 0, 1, 2, 3, 4, k = 0, 1, \dots, K$.

Computational implementation.

In the numerical implementation, the finite generator Q_N is stored as a sparse matrix and the action of the matrix exponential is evaluated numerically as $e^{Q_N^T t}\mathbf{p}(0)$ without explicitly forming the dense matrix exponential. This provides the complete transient probability vector while preserving the coupling among all packet levels and communication phases.

Details of the stationary phase vector.

The steady-state analysis is numerically computed by taking

$$\boldsymbol{\pi} A = 0, \qquad \boldsymbol{\pi}\mathbf{e} = 1, \tag{A17}$$

where

$$\mathbf{e} = [1, 1, 1, 1, 1]^T,$$

letting

$$\begin{aligned} D = {} & \delta_B^3 p + \delta_B^3 q + 2\delta_B^2 \delta_{DB} p + 2\delta_B^2 \delta_{DB} q + 2\gamma_{DF}\delta_B^2 p + \gamma_F \delta_B^2 p \\ & + \delta_B \delta_{DB}^2 p + \delta_B \delta_{DB}^2 q + 3\gamma_{DF}\delta_B \delta_{DB} p + \gamma_{DF}\delta_B \delta_{DB} q \\ & + 4\gamma_F \delta_B \delta_{DB} p + 2\gamma_F \delta_B \delta_{DB} q + 2\delta_B \gamma_{DF}^2 p + 4\gamma_{DF}\gamma_F \delta_B p \\ & + \delta_B \gamma_F^2 p + 2\gamma_F \delta_{DB}^2 p + \gamma_F \delta_{DB}^2 q + 3\gamma_{DF}\gamma_F \delta_{DB} p \\ & + 2\gamma_F^2 \delta_{DB} p + \gamma_F \gamma_{DF}^2 p + 2\gamma_{DF}\gamma_F^2 p + \gamma_F^3 p. \end{aligned} \tag{A18}$$

Then, we obtain

$$\pi_{n,0} = \frac{\delta_B^3 q + 2\delta_B^2 \delta_{DB} q + \delta_B \delta_{DB}^2 q + \gamma_{DF}\delta_B \delta_{DB} q + 2\gamma_F \delta_B \delta_{DB} q + q\delta_{DB}^2 \gamma_F}{D}. \tag{A19}$$

$$\pi_{n,1} = \frac{\delta_B^3 p + 2\delta_B^2 \delta_{DB} p + \delta_B \delta_{DB}^2 p + \gamma_{DF}\delta_B \delta_{DB} p + 2\gamma_F \delta_B \delta_{DB} p + \gamma_F \delta_{DB}^2 p}{D}. \tag{A20}$$

$$\pi_{n,2} = \frac{\begin{array}{c}\gamma_{DF}\delta_B^2 p + \gamma_F \delta_B^2 p + p\delta_B \delta_{DB}\gamma_{DF} + 2p\delta_B\delta_{DB}\gamma_F \\ + p\delta_{DB}^2\gamma_F + p\delta_{DB}\gamma_{DF}\gamma_F + p\delta_{DB}\gamma_F^2\end{array}}{D}. \tag{A21}$$

$$\pi_{n,3} = \frac{\begin{array}{c}p\delta_B^2\gamma_{DF} + p\delta_B\delta_{DB}\gamma_{DF} + p\delta_B\gamma_{DF}^2 + 2p\delta_B\gamma_{DF}\gamma_F \\ + p\delta_B\gamma_F^2 + p\delta_{DB}\gamma_{DF}\gamma_F + p\delta_{DB}\gamma_F^2\end{array}}{D}. \tag{A22}$$

$$\pi_{n,4} = \frac{\begin{array}{c}p\delta_B\gamma_{DF}^2 + 2p\delta_B\gamma_{DF}\gamma_F + p\delta_{DB}\gamma_{DF}\gamma_F \\ + p\gamma_{DF}^2\gamma_F + 2p\gamma_{DF}\gamma_F^2 + p\gamma_F^3\end{array}}{D}. \tag{A23}$$

Transition Entropy Formulation

Consider a relay node in state $(n,3)$. From $(n,3)$, the transitions can go to $(n,1)$, $(n-1,3)$, $(n+1,3)$, accounting for the possible routing for this node. Redefine the probabilities as

$$p_1 = P\big((n,3) \to (n,1)\big),$$

$$p_2 = P\big((n,3) \to (n-1,3)\big),$$

$$p_3 = P\big((n,3) \to (n+1,3)\big).$$

Therefore, the entropy at $(n,3)$ is given by

$$H(n,3) = -\sum_i p_i \log p_i. \tag{A24}$$

Explanation of the Parameter Estimation Formulae

The transition-rate parameters of the proposed CTMC model are estimated from packet event logs using the maximum likelihood estimator (MLE). For each parameter, the numerator represents the total number of observed transitions of a particular type, while the denominator represents the total time spent in the corresponding source state. Hence, the estimated transition rate is expressed as the ratio of the observed transition count to the total state sojourn time.

Arrival Rate λ^j

The arrival rate in phase j is estimated as

$$\hat{\lambda}^j = \frac{\sum_i N_{(i,j),(i+1,j)}}{\sum_i T_{(i,j)}}\ \mathrm{s}^{-1},$$

where $N_{(i,j),(i+1,j)}$ denotes the number of observed transitions from state (i,j) to $(i+1,j)$, corresponding to the arrival of a new packet while remaining in phase j. The quantity $T_{(i,j)}$ represents the total observation time during which the system stays in state (i,j). Thus, $\hat{\lambda}^j$ gives the average packet arrival rate in phase j.

Service Rate μ_j

The service rate is estimated by

$$\hat{\mu}_j = \frac{\sum_i N_{(i,j),(i-1,j)}}{\sum_i T_{(i,j)}}\ \mathrm{s}^{-1},$$

where $N_{(i,j),(i-1,j)}$ is the number of observed packet departures from state (i,j) to $(i-1,j)$, while $T_{(i,j)}$ denotes the cumulative time spent in state (i,j). This estimator represents the average packet service or departure rate during phase j.

Activation Rate p

The packet activation rate is estimated as

$$\hat{p} = \frac{\sum_i N_{(i,0),(i,1)}}{\sum_i T_{(i,0)}} \text{ s}^{-1},$$

where $N_{(i,0),(i,1)}$ denotes the number of transitions from the entry phase to the sensing (active) phase. The denominator $T_{(i,0)}$ is the total time spent in the entry phase. The resulting estimate gives the average rate at which packets become active for sensing or processing.

Return Rate q

The return rate is estimated by

$$\hat{q} = \frac{\sum_i N_{(i,1),(i,0)}}{\sum_i T_{(i,1)}} \text{ s}^{-1},$$

where $N_{(i,1),(i,0)}$ denotes the number of observed transitions from the active phase back to the entry phase and $T_{(i,1)}$ represents the total time spent in the active phase. This estimator gives the average rate at which packets return to the entry state because of deferred sensing, retransmission, or unsuccessful activation.

Notation

The above estimators are standard maximum likelihood estimators for continuous-time Markov chains, where each transition rate is obtained by dividing the total number of observed transitions by the cumulative sojourn time in the corresponding source state.

Table A1. Notation used in the parameter estimation formulae.

Symbol	Description
$N_{(a,b),(c,d)}$	Number of observed transitions from state (a,b) to state (c,d).
$T_{(i,j)}$	Total observation (sojourn) time spent in state (i,j).
$\sum_i$	Summation over all queue levels.
$\hat{\theta}$	Maximum likelihood estimate of parameter θ.
s^{-1}	Unit of the estimated transition rate (per second).

References

1. Yenugula, M. Markov Chain-based Optimization for Efficient and Reliable Wireless Sensor Networks: A Comprehensive Analysis and Enhanced TDMA-CSMA Hybrid Protocol. *Int. J. Comput. Appl.* **2024**, *186*, 7–13. [CrossRef]
2. Deepakraj, D.; Raja, K. Markov-chain based optimization algorithm for efficient routing in wireless sensor networks. *Int. J. Inf. Technol.* **2021**, *13*, 897–904. [CrossRef]
3. Khujamatov, K.; Ahmad, K.; Reypnazarov, E.; Khasanov, D. Markov chain based modeling bandwidth states of the wireless sensor networks of monitoring system. *Int. J. Adv. Sci. Technol.* **2020**, *29*, 4889–4903.
4. Ma, L.; Zhang, N.; Chen, X.; Chen, P.; Yao, Y. A hierarchical traffic offloading mechanism for end-to-end reliability in a multi-hop multi-connection wireless sensor network. *IEEE Sens. J.* **2025**, *25*, 7390–7402. [CrossRef]
5. Jayamani, V.N.; Madheswari, S.P.; Suganthi, P.; Josephine, S.A. An N-policy M/M/1 queueing model for energy saving mechanism in networks. *Sustain. Comput. Inform. Syst.* **2024**, *44*, 101016. [CrossRef]
6. Bhukya, S.N.; Annavarapu, C.S.B. Hybrid reliable clustering algorithm with heterogeneous traffic routing for wireless sensor networks. *Sensors* **2025**, *25*, 864. [CrossRef] [PubMed]
7. Villordo-Jimenez, I.; Torres-Cruz, N.; Menchaca-Mendez, R.; Rivero-Angeles, M.E. Distance-based queueing for scalable and reliable linear wireless sensor networks in smart cities. *Sensors* **2024**, *24*, 2023. [CrossRef] [PubMed]

8. Yang, T.; Sun, J.; Mohajer, A. Queue stability and dynamic throughput maximization in multi-agent heterogeneous wireless networks. *Wirel. Netw.* **2024**, *30*, 3229–3255. [CrossRef]
9. Yang, K. *Wireless Sensor Networks*; Springer: Cham, Switzerland, 2014. [CrossRef]
10. Callaway, E.H. *Wireless Sensor Networks: Architectures and Protocols*; CRC Press: Boca Raton, FL, USA, 2003. [CrossRef]
11. Liu, Y. Wireless sensor network applications in smart grid: Recent trends and challenges. *Int. J. Distrib. Sens. Netw.* **2012**, *8*, 492819. [CrossRef]
12. Arizono, I.; Takemoto, Y. An analysis of steady-state distribution in M/M/1 queueing system with balking based on concept of statistical mechanics. *RAIRO Oper. Res.* **2021**, *55*, S327–S341. [CrossRef]
13. Wang, K.-H.; Chan, M.-C.; Ke, J.-C. Maximum entropy analysis of the $M^{[x]}/M/1$ queueing system with multiple vacations and server breakdowns. *Comput. Ind. Eng.* **2007**, *52*, 192–202. [CrossRef]
14. Kumar, B.K.; Rukmani, R.; Thangaraj, V. On multiserver feedback retrial queue with finite buffer. *Appl. Math. Model.* **2009**, *33*, 2062–2083. [CrossRef]
15. Ammar, S.I. Transient solution of an M/M/1 vacation queue with a waiting server and impatient customers. *J. Egypt. Math. Soc.* **2017**, *25*, 337–342. [CrossRef]
16. Kumar, B.K.; Sankar, R.; Krishnan, R.N.; Rukmani, R.; Rumyantsev, A. Transient and steady-state analysis of hybrid arrivals of single and batch customers queueing systems with switch-off period. *Commun. Stat. Theory Methods* **2023**, *52*, 3382–3413. [CrossRef]
17. Karthick, V.; Suvitha, V.; Sudhesh, R. Transient analysis of two heterogeneous servers queueing system with differentiated vacations subject to system disaster, server repair. *Sankhya B* **2024**, *86*, 751–776. [CrossRef]
18. Rubino, G. Transient analysis of Markovian queueing systems: A survey with focus on closed forms and uniformization. *Queueing Theory* **2021**, *2*, 269–307. [CrossRef]
19. Neuts, M.F. *Matrix-Geometric Solutions in Stochastic Models: An Algorithmic Approach*; Courier Corporation: North Chelmsford, MA, USA, 1994.
20. Latouche, G.; Ramaswami, V. *Introduction to Matrix Analytic Methods in Stochastic Modeling*; Society for Industrial and Applied Mathematics (SIAM): Philadelphia, PA, USA, 1999. [CrossRef]
21. Stewart, W.J. *Probability, Markov Chains, Queues and Simulation: The Mathematical Basis of Performance Modeling*; Princeton University Press: Princeton, NJ, USA, 2009. [CrossRef]
22. Blondia, C. A queueing model for a wireless sensor node using energy harvesting. *Telecommun. Syst.* **2021**, *77*, 335–349. [CrossRef]
23. Kempa, W.M.; Kurzyk, D. On transient queue-size distribution in a model of WSN node with threshold-type power-saving algorithm. *Sensors* **2022**, *22*, 9285. [CrossRef] [PubMed]
24. Blondia, C. Evaluation of the end-to-end response times in an energy harvesting wireless sensor network using a receiver-initiated MAC protocol. *Ad Hoc Netw.* **2022**, *136*, 102971. [CrossRef]
25. Abbad, L.; Nacer, A.; Abbad, H.; Brahim, M.T.; Zioui, N. A weighted Markov-clustering routing protocol for optimizing energy use in wireless sensor networks. *Egypt. Inform. J.* **2022**, *23*, 483–497. [CrossRef]
26. Affane, A.R.; Satori, H.; Sanhaji, F.; Boutazart, Y.; Satori, K. Energy enhancement of routing protocol with hidden Markov model in wireless sensor networks. *Neural Comput. Appl.* **2023**, *35*, 5381–5393. [CrossRef]
27. Dudin, A.; Klimenok, V. Analysis of MAP/G/1 queue with inventory as the model of the node of wireless sensor network with energy harvesting. *Ann. Oper. Res.* **2023**, *331*, 839–866. [CrossRef]
28. Zhang, C.; Yang, J.; Wang, N. Timely reliability modeling and evaluation of wireless sensor networks with adaptive *N*-policy sleep scheduling. *Reliab. Eng. Syst. Saf.* **2023**, *235*, 109270. [CrossRef]
29. Zhang, C.; Yang, J.; Wang, N. An active queue management for wireless sensor networks with priority scheduling strategy. *J. Parallel Distrib. Comput.* **2024**, *187*, 104848. [CrossRef]
30. Shudrenko, Y.; Timm-Giel, A. Modeling end-to-end delays in TSCH wireless sensor networks using queuing theory and combinatorics. *Computing* **2024**, *106*, 2923–2947. [CrossRef]
31. Kumar, A.; Jadhav, S.; Alsalami, O.M. Reliability and sensitivity analysis of wireless sensor network using a continuous-time Markov process. *Mathematics* **2024**, *12*, 3057. [CrossRef]
32. Singh, A.; Yadav, P.; Kulshrestha, R.; Kumar, A. Transient and Multi-Objective Analysis for Energy Efficient, Unreliable CRN with Hybrid Spectrum Access and Imperfect Sensing. *Arab. J. Sci. Eng.* **2026**, *51*, 1–23. [CrossRef]
33. Champati, J.P.; Al-Zubaidy, H.; Gross, J. Transient Analysis for Multihop Wireless Networks under Static Routing. *IEEE/ACM Trans. Netw.* **2020**, *28*, 722–735. Available online: https://ieeexplore.ieee.org/document/9036049 (accessed on 18 October 2026). [CrossRef]
34. Sudhesh, R.; Mohammed Shapique, A. Transient Analysis of Power Management in Wireless Sensor Network with Start-Up Times and Threshold Policy. *Telecommun. Syst.* **2022**, *80*, 1–16. [CrossRef]

35. Bayan, N.; Erfani, S. Laplace Transform Approach to Analysis and Synthesis of Bessel Type Linear Time-Varying Systems. In Proceedings of the 2007 50th Midwest Symposium on Circuits and Systems, Montreal, QC, Canada, 5–8 August 2007; IEEE: Piscataway, NJ, USA, 2007; pp. 919–923. Available online: https://ieeexplore.ieee.org/document/4488718 (accessed on 18 October 2026).
36. Singh, C.J.; Jain, M.; Kaur, S. Performance analysis of bulk arrival queue with balking, optional service, delayed repair and multi-phase repair. *Ain Shams Eng. J.* **2018**, *9*, 2067–2077. [CrossRef]
37. Mandjes, M.; Sollie, B. A numerical approach for evaluating the time-dependent distribution of a quasi birth-death process. *Methodol. Comput. Appl. Probab.* **2022**, *24*, 1693–1715. [CrossRef]
38. Park, P.; Di Marco, P.; Fischione, C.; Johansson, K.H. Modeling and optimization of the IEEE 802.15.4 protocol for reliable and timely communications. *IEEE Trans. Parallel Distrib. Syst.* **2012**, *24*, 550–564. [CrossRef]

Disclaimer/Publisher's Note: The statements, opinions and data contained in all publications are solely those of the individual author(s) and contributor(s) and not of MDPI and/or the editor(s). MDPI and/or the editor(s) disclaim responsibility for any injury to people or property resulting from any ideas, methods, instructions or products referred to in the content.